A bacterial phytochrome-based optogenetic system controllable with near-infrared light

Andrii A Kaberniuk, Anton A Shemetov & Vladislav V Verkhusha

Light-mediated control of protein–protein interactions to regulate cellular pathways is an important application of optogenetics. Here, we report an optogenetic system based on the reversible light-induced binding between the bacterial phytochrome BphP1 and its natural partner PpsR2 from *Rhodopseudomonas palustris* bacteria. We extensively characterized the BphP1–PpsR2 interaction both *in vitro* and in mammalian cells and then used this interaction to translocate target proteins to specific cellular compartments, such as the plasma membrane and the nucleus. We showed light-inducible control of cell morphology that resulted in a substantial increase of the cell area. We demonstrated light-dependent gene expression with 40-fold contrast in cultured cells, 32-fold in subcutaneous mouse tissue, and 5.7-fold in deep tissues in mice. Characteristics of the BphP1–PpsR2 optogenetic system include its sensitivity to 740- to 780-nm near-infrared light, its ability to utilize an endogenous biliverdin chromophore in eukaryotes (including mammals), and its spectral compatibility with blue-light-driven optogenetic systems.

Spatiotemporal control of biochemical processes in cells and animals achieved through techniques such as optogenetics can help advance research in basic biology and biomedicine. An important avenue of optogenetic manipulation is the modulation of cellular protein–protein interactions (PPIs). Genetically encoded light-dependent systems exhibit several advantages over pharmacologically inducible PPI approaches because of their noninvasiveness, high PPI activation rates, reversibility, and lack of side effects potentially caused by drugs.

PPI optogenetic systems[1] were engineered from different photoreceptor families including LOV (light–oxygen–voltage) domain proteins[2,3], BLUF (blue light using FAD) domain proteins[4], cryptochromes[5,6], and plant phytochromes[7–9]. The application of these optogenetic tools in mammals is complicated by their dependence on short-wavelength illumination outside of the near-infrared (NIR) tissue transparency window between 650 and 900 nm[10]. An exception is the phytochrome family, which is activated with far-red or NIR light. Phytochromes require the incorporation of tetrapyrrole chromophores. Phytochromobilin and phycocyanobilin serve as chromophores in plant phytochromes, whereas bacterial phytochromes incorporate biliverdin IXα (BV)[11,12]. Among these tetrapyrroles, BV exhibits the most NIR-shifted absorbance spectra. While plant phytochrome-based optogenetic systems require an exogenous supply of phycocyanobilin[13], the BV chromophore used by bacterial phytochromes is abundant in eukaryotic cells[14]. Therefore, bacterial phytochromes have been engineered into several types of NIR probes for mammalian tissues[15], including constitutively fluorescent proteins[16,17], photoactivatable fluorescent proteins[18], and PPI reporters[19].

Bacterial phytochromes control gene expression and second messenger signaling in bacteria in response to NIR light[20]. These phytochromes consist of a photosensory core module and an output effector module. Natural output modules have been replaced with phosphodiesterase and adenylate cyclase, enabling the manipulation of cyclic nucleotides in mammalian cells[21–23]. Spectral properties of bacterial phytochromes are defined by a photosensory core module where the protein–chromophore interaction occurs[11,24,25]. Within the chromophore-binding pocket, BV can adopt two conformational states, Pr and Pfr, which absorb far-red and NIR light, respectively. Most bacterial phytochromes undergo photoconversion from the Pr state to the Pfr state when exposed to 660- to 700-nm light. However, there is a small group, termed 'bathy phytochromes', that adopts Pfr as a ground state and undergoes Pfr→Pr photoconversion with 740- to 780-nm light[26]. Bacterial phytochromes can be converted back to a ground state either with light or through thermal relaxation in darkness.

The effector module of the bacterial bathy phytochrome RpBphP1 (BphP1) from *R. palustris* consists of two domains, PAS/PAC (PAS domain with additional C-terminal residues) and HOS (2-helix output sensor), and has no detectable enzymatic activity. It has been proposed that BphP1 performs its signaling function by interacting with the transcriptional repressor RpPpsR2 upon NIR illumination[27]. While a light-induced BphP1–RpPpsR2 heterodimerization was observed by gel filtration, it was not characterized further[28].

In this paper, we study the light-activatable interaction of BphP1 with RpPpsR2 *in vitro* and *in vivo*. We demonstrate recruitment of one of the interacting partners to specific cellular compartments and utilize this recruitment to induce intracellular signaling and

Department of Anatomy and Structural Biology, Albert Einstein College of Medicine, Bronx, New York, USA. Correspondence should be addressed to V.V.V. (vladislav.verkhusha@einstein.yu.edu).

RECEIVED 6 JULY 2015; ACCEPTED 10 APRIL 2016; PUBLISHED ONLINE 9 MAY 2016; DOI:10.1038/NMETH.3864

to control gene expression. We show that the BphP1–RpPpsR2 pair can be used as a PPI-inducing NIR optogenetic system that is facilitated by the presence of endogenous BV in mammalian cells and animals.

RESULTS

Properties of purified BphP1

In its ground Pfr state, BphP1 absorbs maximally at 412 nm (Soret band) and at 756 nm (Q band) (**Fig. 1a**). Upon NIR illumination, BphP1 photoconverts into the Pr state with absorbance at 390 nm and 678 nm for Soret and Q bands, respectively. We observed a 4.3-fold decrease in absorbance at 756 nm upon 740/25-nm irradiation (**Supplementary Table 1**). The highest light sensitivity of the Pfr state was observed at ~740–780 nm, with notable BphP1 photoconversion occurring at 800 nm (**Fig. 1b**). Kinetics of the Pfr→Pr photoconversion was monoexponential (**Supplementary Fig. 1a**). The half-time of the Pfr→Pr transition was 28 s at 1 mW cm^{-2}, and it decreased to 3.5 s at 27 mW cm^{-2} (**Fig. 1c**). After the Pfr→Pr photoconversion, BphP1 returned to the ground state in darkness with a half-time of 170 s. BphP1 could undergo repeated cycles of Pfr→Pr photoconversion followed by dark relaxation back to the Pfr state (**Fig. 1d**). Irradiation with 636-nm light restored Pfr absorbance to ~80% (**Fig. 1a**). The remaining ~20% of Pfr absorbance was restored during dark relaxation (**Supplementary Fig. 1b**). The half-time of the Pfr→Pr conversion depended on the 636-nm light intensity, ranging from 21 s at 1 mW cm^{-2} to 3.0 s at 45 mW cm^{-2} (**Fig. 1e**). Multiple cycles of photoswitching did not lead to notable changes in absorbance (**Fig. 1f**).

BphP1–PpsR2 interaction *in vitro*

RpPpsR2 has a single cysteine residue in position 439 and forms a noncovalent homodimer. To exclude the possibility of disulfide bond formation, we substituted cysteine 439 with serine and named this RpPpsR2-C439S variant PpsR2. We then fused mRuby2 to the C terminus of PpsR2 and characterized the BphP1–PpsR2 interaction using FRET. mRuby2 emission and BphP1 absorbance in the Pr state have good spectral overlap (**Supplementary Fig. 2a**), resulting in quenching of mRuby2 fluorescence (**Supplementary Fig. 2b**). 740-nm light caused an increase in the Pr state, and the BphP1–PpsR2-mRuby2 binding caused up to a 12% decrease in mRuby2 fluorescence. A 27-fold change in 740-nm light intensity did not cause changes in the kinetics of the mRuby2 fluorescence decrease (**Supplementary Fig. 2c**). For all intensities tested, the fluorescence quenching exhibited a half-time of ~60 s, which was larger than that observed for BphP1 alone (**Fig. 1c**). This suggested that PpsR2 did not bind BphP1 in the Pfr state, and that the BphP1–PpsR2 interaction was not limited by the rate of Pfr→Pr photoconversion but rather by BphP1 and/or PpsR2 structural changes involved in the interaction.

Using 740 nm for the Pfr→Pr and 636 nm for the Pr→Pfr photoconversion, we monitored several cycles of FRET changes (**Fig. 1g**) with half-times of ~60 s and ~30 s, respectively (**Supplementary Table 1**). The observed incomplete Pr→Pfr switching with 636-nm light could have been caused by overlap of the Pr and Pfr spectra at this wavelength (**Fig. 1a**). Dark relaxation in the BphP1–PpsR2 complex was slower than photoswitching with 636 nm and depended on the BphP1:PpsR2 ratio, with shorter half-times of

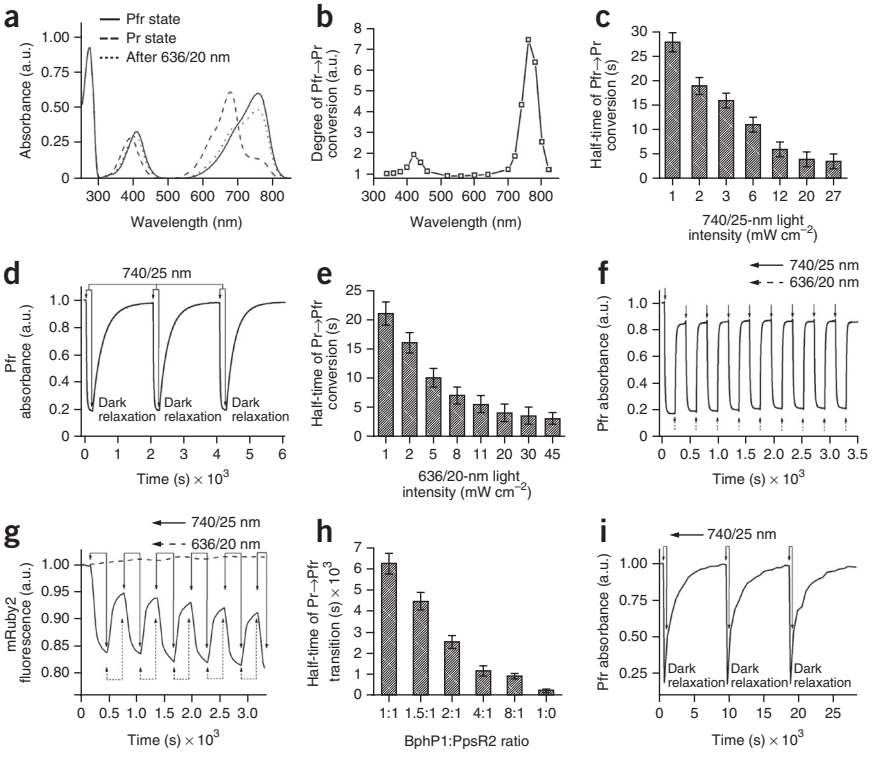

Figure 1 | Spectral properties of BphP1 and characterization of BphP1–PpsR2 interaction *in vitro*. (**a**) Absorbance spectra of BphP1 in the Pfr state (solid line), after photoconversion to the Pr state with 740/25 nm (dashed line), and after conversion back to the Pfr state with 636/20 nm (dotted line). (**b**) Action spectrum of the Pfr→Pr photoconversion measured as the relative decrease of Pfr absorbance detected at 780 nm upon irradiation with light of specific wavelength. (**c**) Dependence of the half-time of light-induced Pfr→Pr photoconversion on the intensity of 740/25-nm light (n = 3, error bars are s.e.m.). (**d**) Absorbance of BphP1 in the Pfr state during repeated illumination with 740/25-nm light followed by dark relaxation. (**e**) Dependence of the half-time of light-induced BphP1 Pr→Pfr photoconversion on the intensity of 636/20-nm light (n = 3, error bars are s.e.m.). (**f**) Absorbance of BphP1 in the Pfr state during repeated illumination cycles with 740/25-nm light and then with 636/20-nm light. Absorbance in **b**, **d**, and **f** was measured at 780 nm. (**g**) Time course of FRET changes during BphP1 photoswitching between the Pr and Pfr states either together with PpsR2-mRuby2 (solid line) or together with mRuby2 control (dashed line). Solid arrows correspond to 740/25-nm illumination. Dashed arrows correspond to 636/20-nm illumination. (**h**) Half-time of dark relaxation of BphP1 (Pr→Pfr transition) in the presence of various quantities of PpsR2-mRuby2 (n = 3, error bars are s.e.m.). (**i**) Reversible dark relaxation cycles from the Pr to the Pfr state of a BphP1 and PpsR2 mixture with an 8:1 ratio. Arrows correspond to 740/25-nm illumination.

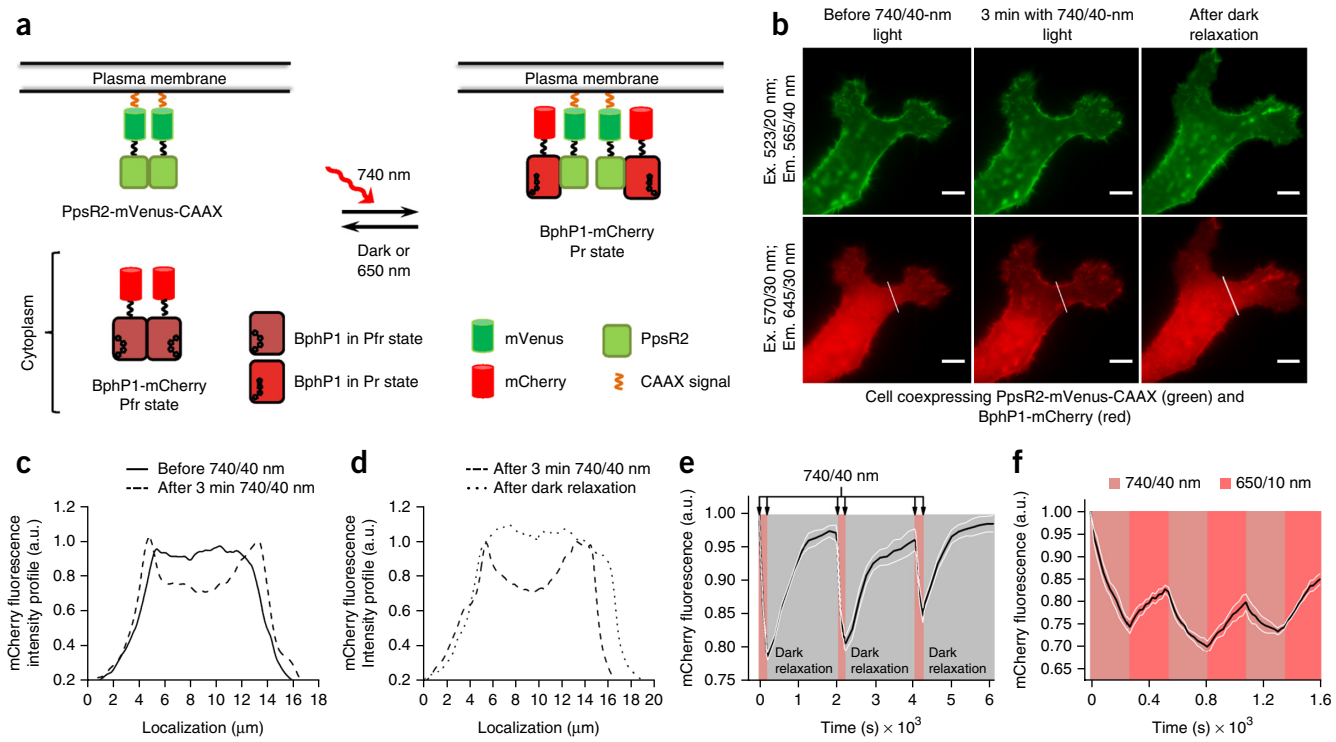

Figure 2 | Light-induced relocalization of BphP1 to the plasma membrane. (**a**) A model for the light-induced interaction between cytoplasmic BphP1-mCherry and membrane-bound PpsR2-mVenus-CAAX. (**b**) Fluorescence images of a HeLa cell coexpressing PpsR2-mVenus-CAAX (green) and BphP1-mCherry (red) before illumination (left), after 3 min of 740/40-nm illumination with 0.9 mW cm^{-2} (middle), and after 20 min of dark relaxation (right). Ex., excitation filter; em., emission filter. Bars, 10 μm. (**c**) Intensity profile of BphP1-mCherry fluorescence of the cell in **b** marked with a white line before (solid line) and after (dashed line) 3 min of 740/40-nm illumination. (**d**) Intensity profile of BphP1-mCherry fluorescence of the cell in **b** marked with a white line after 3 min of 740/40-nm illumination (dashed line) and after subsequent 24 min in darkness (dotted line). (**e**) Time course of BphP1-mCherry fluorescence intensity in the cytoplasm during three cycles of 3 min of 740/40-nm irradiation with 0.2 mW cm^{-2} followed by 30 min in darkness ($n = 5$; white lines represent mean ± s.e.m.). mCherry fluorescence was measured every 15 s during 740/40-nm light illumination and every 180 s during dark relaxation. (**f**) Time course of the BphP1-mCherry fluorescence intensity in the cytoplasm during three cycles of 3 min of 740/40-nm irradiation with 0.2 mW cm^{-2} followed by 3 min of 650/10-nm irradiation with 0.35 mW cm^{-2} ($n = 5$; white lines represent mean ± s.e.m.). mCherry fluorescence was measured every 15 s. All imaging was performed at 37 °C using an epifluorescence microscope. Light intensities were measured at the back focal plane of a 60×, 1.35 numerical aperture (NA) objective lens.

Pr→Pfr dark relaxation (as detected by Pfr absorbance) corresponding to the larger BphP1 concentrations (**Fig. 1h**). The dark relaxation half-time was 900 s (**Supplementary Table 1**), suggesting that the BphP1–PpsR2 binding substantially slowed the Pr→Pfr relaxation and BphP1–PpsR2 dissociation in darkness. After complete dark relaxation the complexes can be formed again by 740-nm light illumination (**Fig. 1i**).

BphP1–PpsR2 interaction in mammalian cells

To study the BphP1–PpsR2 interaction in mammalian cells we used a translocation assay (**Fig. 2a**). We fused PpsR2 with mVenus and a CAAX plasma membrane localization signal, and we fused BphP1 with mCherry for cytoplasmic expression. Excitation of these fluorescent proteins did not photoconvert BphP1 (**Supplementary Fig. 3**). Illumination of HeLa cells with 740-nm light caused the translocation of BphP1-mCherry to the plasma membrane and a 25% decrease in mCherry cytoplasmic intensity after 3 min of 740-nm illumination detected with an epifluorescence microscope (**Fig. 2b**,**c**). Subsequent dark incubation restored BphP1-mCherry fluorescence in the cytoplasm to the original level in ~24 min (**Fig. 2b**,**d**). We demonstrated the reversibility of the BphP1 translocation to the plasma membrane and back to the cytoplasm for three cycles of 3 min of 740-nm illumination followed by 30 min of dark relaxation (**Fig. 2e**), with the recovery of ~95% of the initial mCherry cytoplasmic intensity. Then we studied the effect of 650-nm light on acceleration of the BphP1 dissociation from the plasma membrane and found a 1.6-fold higher initial rate of BphP1-mCherry cytoplasmic signal recovery compared to the initial rate in darkness (**Supplementary Fig. 4**). However, complete dissociation of the BphP1–PpsR2 complexes required darkness. Illumination with 740- and 650-nm light for 3 min each resulted in ~8% reversible changes of the BphP1-mCherry cytoplasmic signal after the initial 25% decrease (**Fig. 2f**), indicating that one-third of the BphP1–PpsR2 complexes could be modulated with light.

Light-induced activation of a signaling pathway

We next used the BphP1–PpsR2 interaction for the recruitment of a DHPH domain of intersectin 1 (ref. 29) to the plasma membrane for activation of the small GTPase Cdc42 (refs. 30,31). We fused the DHPH domain to the C terminus of BphP1-mCherry and coexpressed the construct in HeLa cells with PpsR2-mVenus-CAAX (**Fig. 3a**). 740-nm illumination caused changes to cell morphology and a gradual increase of the cell area with a plateau after ~30 min (**Fig. 3b**). We did not detect any notable changes in cells cotransfected with BphP1-mCherry-DHPH and

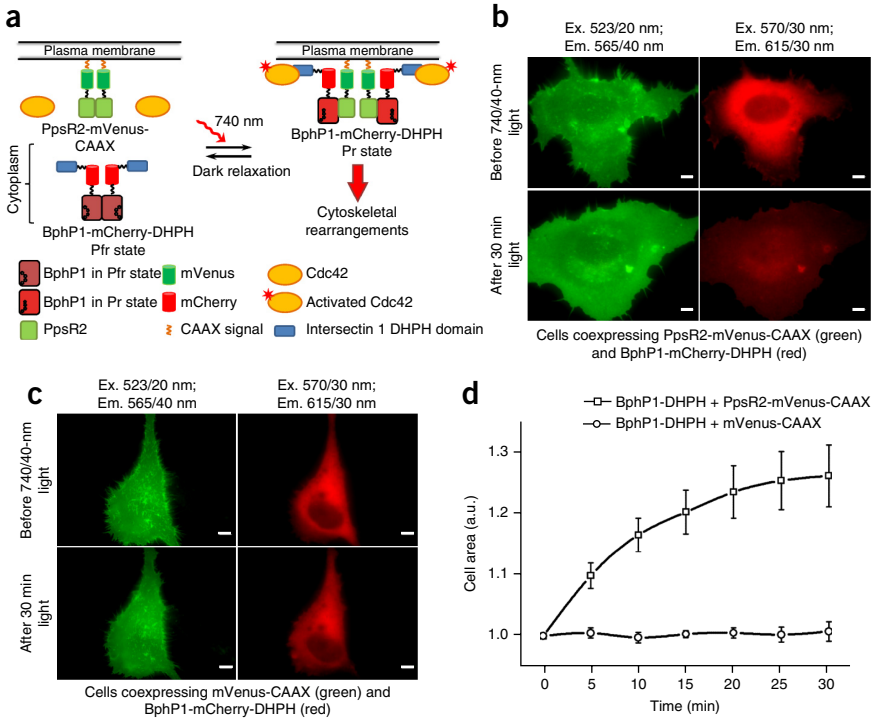

Figure 3 | Light induction of cellular cytoskeletal rearrangements. (**a**) A model for the light-induced recruitment of cytoplasmic BphP1-mCherry-DHPH to membrane-bound PpsR2-mVenus-CAAX that results in cytoskeletal rearrangements of mammalian cells. (**b**,**c**) Fluorescence images of HeLa cells coexpressing either (**b**) BphP1-mCherry-DHPH (red) and PpsR2-mVenus-CAAX (green) or (**c**) BphP1-mCherry-DHPH (red) and mVenus-CAAX control (green) before (top) and after (bottom) 30 min irradiation with 740/40-nm light of 0.2 mW cm^{-2} (first 3 min continuous irradiation with 740/40-nm followed by 27 min of pulse illumination 15 s On 45 s Off). Ex., excitation filter; Em., emission filter. Bars, 10 µm. (**d**) Time-dependent size changes of HeLa cells coexpressing either BphP1-mCherry-DHPH and PpsR2-mVenus-CAAX ($n = 5$; error bars are s.e.m.) or BphP1-mCherry-DHPH and mVenus-CAAX control ($n = 5$; error bars are s.e.m.) during irradiation with 740/40-nm light of 0.2 mW cm^{-2} (first 3 min continuous irradiation with 740/40-nm followed by 27 min of pulsed illumination 15 s On and 45 s Off). Fluorescent images were taken every 15 s during continuous irradiation and every 60 s during pulsed irradiation with 740/40 nm. All imaging was performed at 37 °C using an epifluorescence microscope. The light power densities were measured at the back focal plane of a 60×, 1.35 NA objective lens.

mVenus-CAAX (**Fig. 3c**). In the former cotransfection, the area increased up to 50% in some cells, with an average increase of ~25% (**Fig. 3d**). The initial relative decrease of BphP1-mCherry-DHPH in the cytoplasm was two-fold higher than the cell area increase, indicating that BphP1-mCherry-DHPH translocated mainly during the first 5 min of 740-nm irradiation. Further changes were similar for mCherry fluorescence and cell area, suggesting that these changes were caused by an increase in the cell area (**Supplementary Fig. 5**).

BphP1 recruitment to the cell nucleus

To examine whether we could optogenetically induce nuclear import, we transfected HeLa cells that stably expressed BphP1-mCherry with PpsR2-mVenus containing a nuclear localization signal (NLS). In darkness, NLS-PpsR2-mVenus localized to the nucleus, and BphP1-mCherry stayed in the cytoplasm (**Fig. 4a**), with an mCherry intensity ratio between the nucleus and the cytoplasm of ~0.5 (**Supplementary Fig. 6**). 740-nm illumination caused an increase of BphP1-mCherry fluorescence in the nucleus (**Fig. 4a**), resulting in a nucleus:cytoplasm ratio of 1.8. Cells expressing only BphP1-mCherry displayed nucleus:cytoplasm ratios below 0.5, both in darkness and after illumination (**Supplementary Fig. 6**). Thus, the light-induced BphP1-PpsR2 interaction caused an ~3.5-fold increase of the BphP1-mCherry signal in nuclei of illuminated cells.

A light-inducible TetR–*tetO* transcription system

To develop a light-inducible transcription system, we combined the light-induced recruitment of BphP1 to the nucleus with a tetracycline-repressor-based system (**Fig. 4b**). We fused VP16 to the C terminus of NLS-PpsR2 and the tetracycline repressor (TetR) (ref. 32) to BphP1-mCherry. We cotransfected HeLa cells stably expressing BphP1-mCherry-TetR with a plasmid encoding NLS-PpsR2-VP16 and with a pTRE–Tight–SEAP plasmid containing seven copies of *tetO* (7× *tetO*) upstream of the *SEAP* gene. 740-nm illumination increased SEAP levels ~40-fold over the levels in darkness after 48 h (**Supplementary Fig. 7a**,**b**). The time course of SEAP production revealed an ~14-fold increase in SEAP after 12 h of 740-nm illumination compared to that in dark-treated cells (**Supplementary Fig. 7c**). SEAP accumulation exhibited a half-time of ~18 h and reached a plateau after 48 h (**Fig. 4c** and **Supplementary Fig. 7c**). SEAP expression level depended on the power of activating light, with SEAP signal observed in cells irradiated with as little as 0.05 mW cm^{-2} (**Supplementary Fig. 8**). Similarly, the light-induced BhpP1–PpsP2 interaction that caused EGFP expression from a pTRE–Tight–EGFP reporter plasmid resulted in more than 27-fold greater EGFP signal in illuminated cells over dark-treated cells as detected by flow cytometry (**Supplementary Fig. 9**).

We next studied how fast the light-induced transcriptional activation could be terminated. We illuminated cells with 740-nm light for 12 h and then kept them in darkness. The SEAP reporter production increased ~2.6-fold during the first 12 h in darkness (likely because of preaccumulation of SEAP mRNA) and subsequently decreased with a half-time of ~8 h (**Fig. 4d**). We tested whether 636-nm light would accelerate the termination of transcriptional activation and found that 12 h illumination at 636 nm after the 12-h illumination period with 740-nm light decreased the SEAP production ~2.3-fold compared to the cells kept in darkness. Moreover, the SEAP decrease in the subsequent darkness after 636-nm illumination was also ~2-fold faster (**Fig. 4d**). Thus, similar to cell membrane relocalization (**Fig. 2**),

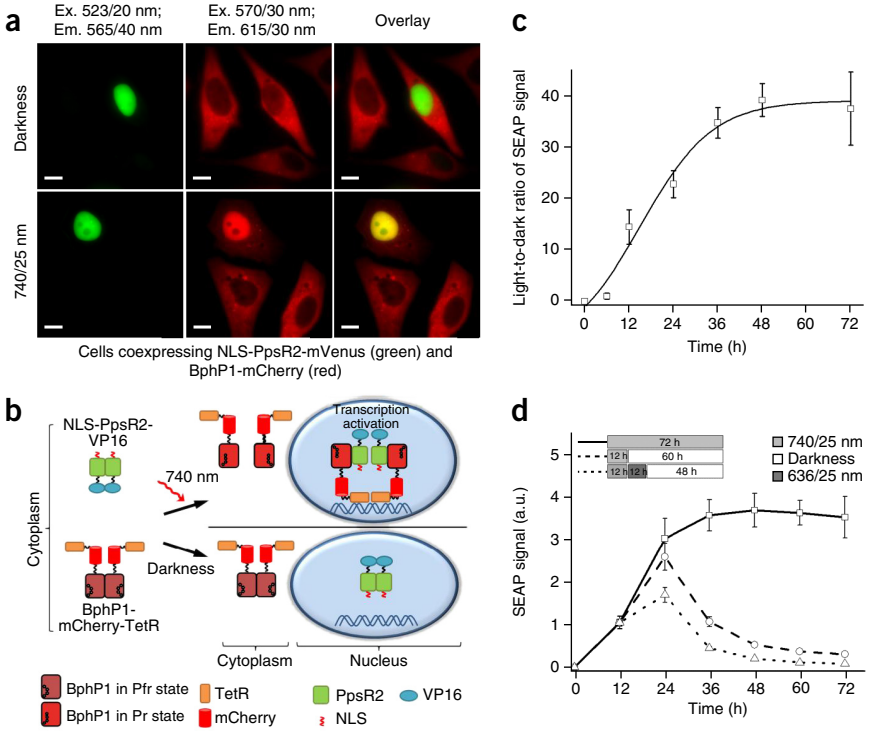

Figure 4 | Recruitment of BphP1 to the nucleus and light-induced transcription activation. (**a**) Fluorescence images of HeLa cells coexpressing NLS-PpsR2-mVenus and BphP1-mCherry incubated either in darkness or under irradiation with 740/25-nm pulsed light (30 s On and 180 s Off) of 0.2 mW cm^{-2}. Images were acquired at 37 °C using an epifluorescence microscope. Pseudocolor images (mVenus channel in green and mCherry channel in red) and their overlay are shown. Ex., excitation filter; em., emission filter. Bars, 10 µm. (**b**) Model of the light-inducible transcription activation system. NIR light converts BphP1 into the Pr state and induces heterodimerization with PpsR2. NLS fused with PpsR2 facilitates translocation of the heterodimer to the nucleus where BphP1 fusions interact with *tet0* DNA repeats via fused TetR. VP16 fused with PpsR2 recruits the transcription initiation complex and triggers transcription of a reporter gene. (**c**) Kinetics of the light-to-dark ratio of SEAP signal detected in culture media of HeLa cells bearing BphP1-mCherry-TetR cotransfected with NLS-PpsR2-VP16-producing plasmid and pTRE–Tight–SEAP (7× *tet0*) reporter plasmid after 48 h (n = 3; error bars are s.e.m.). (**d**) Termination of SEAP transcription in HeLa cells with the same constructs as in **c** illuminated with 740/25 nm followed by 60 h of darkness or followed by 12 h of 636/25-nm illumination and then by 48 h of darkness. Data were normalized to SEAP signal of cells irradiated with 740/25 nm for 72 h; the signal from nonirradiated cells was subtracted (n = 3; error bars are s.e.m.).

the termination of gene transcription can be accelerated with 636-nm illumination, which causes dissociation of the BphP1-TetR and PpsR2-VP16 complexes in a nucleus.

We next compared two similar TetR–*tetO* transcription activation systems, one based on the BphP1–PpsR2 pair and another on a PhyB–PIF6 pair[13], using the same reporter plasmid. The reporter expression was two-fold higher for the BphP1–PpsR2 than for the PhyB–PIF6 interaction (**Supplementary Fig. 10**). Comparison of light propagation for 660- and 740-nm wavelengths in various mammalian tissues revealed a substantially more effective penetration of NIR light (**Supplementary Note** and **Supplementary Fig. 11**), resulting in higher reporter expression at greater tissue depth for the BphP1–PpsR2 system compared to the PhyB–PIF6 system (**Supplementary Fig. 12**).

Light activation of gene expression *in vivo*

For activation of gene expression *in vivo*, we cotransfected stably expressing BphP1-mCherry-TetR HeLa cells with NLS-PpsR2-VP16 and pTRE–Tight–Rluc8 plasmids and subcutaneously injected the cells into the interscapulum area of FVB mice 24 h after cotransfection. Then, we either illuminated the animals with 740-nm light or kept them in darkness. After 48 h we detected a substantial increase of the Rluc8 signal in the illuminated mice (**Fig. 5a**) as compared to those kept in darkness. The observed 32-fold activation contrast (**Fig. 5b**) was similar to that obtained in cell culture experiments (**Supplementary Fig. 7b**).

We further compared the BphP1–PpsR2 system with a blue-light-activated LightON system[33]. In cultured cells, LightON activation with 470-nm light resulted in a 42-fold increase of the Rluc8 signal over the signal in dark-treated cells (**Supplementary Fig. 13**). However, experiments with subcutaneously injected cells in FVB mice led to only a 15-fold Rluc8 activation contrast (**Fig. 5c,d**). This 2.8-fold drop in Rluc8 production in the LightON system was likely caused by the higher absorbance of 470-nm as compared to 740-nm light by ~1-mm-thick tissue.

To determine whether both the LightON and our system could potentially be used concurrently, we tested for optical crosstalk in cell culture. Activation of both systems in cultured cells with 470-nm and 740-nm light revealed their low crossactivation. We detected 12-fold higher activation of the LightON system with 470-nm light and 18-fold higher activation of the BphP1–PpsR2 system with 740-nm light (**Supplementary Fig. 14**).

For deep tissue studies, we assessed the kinetics of light-induced Rluc8 expression in mice after hydrodynamic transfection (**Fig. 5e–h** and **Supplementary Fig. 15**). After 24 h we detected an increase of Rluc8 signal in livers of 740-nm-illuminated mice in comparison with the dark-treated animals (**Fig. 5f**). After 48 h the Rluc8 signal reached its maximum with a 5.7-fold light-to-dark signal ratio (**Fig. 5e,f**). Large differences of Rluc8 expression between the illuminated and dark-treated animals were observed up to 72 h after transfection (**Fig. 5f**). To test the LightON system, we hydrodynamically transfected mice either with the large amounts of the LightON and reporter plasmids used in the original paper[33] (**Supplementary Fig. 15**) or with amounts similar to those of the BphP1–PpsR2 system (**Fig. 5g,h**). In the former case, after 470-nm illumination of mice for 24 h we observed a 1.7-fold increase of the Rluc8 production as compared to the dark-treated animals. In the latter case, the signal increase was 2.8-fold (**Fig. 5g,h**), which was one-half of that detected for the BphP1–PpsR2 system (**Fig. 5e,f**). The Rluc8 'bell-shaped' kinetics of the LightON activation in liver observed in both conditions was similar to that reported[34].

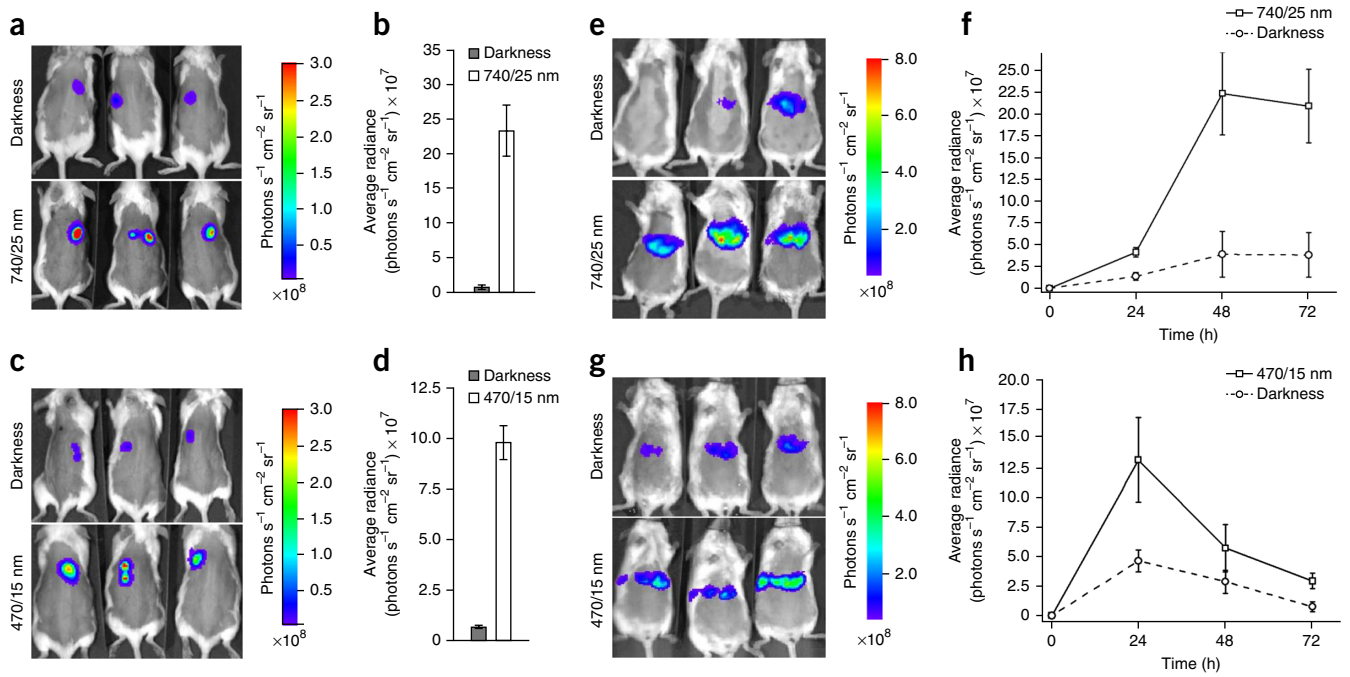

Figure 5 | Light-induced transcription activation in mice. (**a**) Rluc8 bioluminescence detected in mice with subcutaneously injected HeLa cells stably expressing BphP1-mCherry-TetR and cotransfected with the NLS-PpsR2-VP16-producing plasmid and pTRE–Tight–Rluc8 reporter plasmid kept either in darkness (top) or illuminated with 740/25-nm light of 1 mW cm^{-2} (bottom) for 48 h. (**b**) Rluc8 signals detected in dark-treated animals and in illuminated animals shown in **a** ($n = 3$; error bars are s.e.m.). (**c**) Rluc8 signals in mice with subcutaneously injected HeLa cells cotransfected with pGAVPO-plasmid-encoding GAL4(65)-VVD-p65 activation domain and pU5–Rluc8 reporter plasmid kept in darkness (top) or illuminated with 470/15-nm light of 1 mW cm^{-2} (bottom) for 48 h. (**d**) Rluc8 signals detected in the dark-treated and illuminated animals shown in **c** ($n = 3$; error bars are s.e.m.). (**e**) Rluc8 signals detected in mice after hydrodynamic cotransfection with pKA–207I10 (encoding NLS-PpsR2-VP16-IRESv10-BphP1-mCherry-VP16) (50 µg) and pTRE–Tight–Rluc8 (5 µg) plasmids. Mice kept in darkness (top) or illuminated with 740/25-nm light of 5 mW cm^{-2} (bottom) for 48 h. (**f**) Kinetics of the Rluc8 expression in mice shown in **e** kept in darkness or illuminated for 72 h ($n = 3$; error bars are s.e.m.). (**g**) Rluc8 signals detected in mice after hydrodynamic cotransfection with pGAVPO (50 µg) and pU5–Rluc8 (5 µg) plasmids. Mice kept in darkness (top) or illuminated with 470/15-nm light of 5 mW cm^{-2} (bottom) for 24 h. (**h**) Kinetics of Rluc8 expression in mice shown in **g** kept in darkness or illuminated for 72 h ($n = 3$; error bars are s.e.m.).

DISCUSSION

We have developed a novel optogenetic system based on the light-inducible interaction of bacterial phytochrome BphP1 and its binding partner PpsR2 from *R. palustris*. This system takes advantage of the high sensitivity of bacterial phytochromes to NIR light and their unique ability to incorporate heme-derived BV as a chromophore. The BphP1–PpsR2 optogenetic system can be used to activate several types of cellular processes. We showed the light-induced recruitment of cytoplasmic BphP1 to membrane-bound PpsR2 and used this approach to activate the Cdc42 signaling pathway.

We extended the light-induced targeting approach to the recruitment of BphP1 to a nucleus and developed the transcription activation system. The light-induced transcription was reversible in darkness, while far-red illumination accelerated the transcription termination two-fold, allowing its more precise control. The implementation of our optogenetic tool as an NIR-light-inducible transcription system should enable protein expression in a spatiotemporally controlled manner in other model organisms that are compatible with the TetR–*tetO* (ref. 35) interaction. This light-inducible, tetracycline-independent, TetR-based system will allow researchers to avoid potential drawbacks associated with tetracycline consumption by experimental animals[36].

For *in vivo* applications, optogenetic systems sensing NIR light are preferable because of their deep tissue penetration and low phototoxicity. The majority of far-red optogenetic systems are based on a PPI between plant phytochrome PhyB and the PIF6 factor[8,13,37]. They are activated with far-red light peaked at 660 nm, whereas BphP1–PpsR2 interaction is activated with NIR 740- to 780-nm light (**Fig. 1b**). Moreover, the use of the PhyB–PIF6 system is limited by the requirement either to supply an exogenous phycocyanobilin chromophore[11,12] or to produce it by coexpressing several bacterial enzymes[38], thereby affecting cellular metabolism.

Our *in vivo* comparison of transcription activation by the blue-light-driven LightON system and the NIR-light-activated BphP1–PpsR2 system revealed a higher efficiency of the latter system at light intensities of ≤5 mW cm^{-2}, which are compliant with safety regulations[39]. These light intensities caused a smaller increase of the Rluc8 signal in a deep-seated liver in the 470-nm-illuminated animals as compared with the Rluc8 signal obtained with 90 mW cm^{-2} illumination used in the original LightON paper[33].

In summary, we have characterized the BphP1–PpsR2 light-controllable PPI *in vitro* and in cells and animals, and we have demonstrated the use of this light-sensitive pair as an optogenetic system for subcellular protein targeting, induction of intracellular enzymatic activity, and activation of gene expression. The BphP1–PpsR2 system is orthogonal to mammalian cells and minimally interferes with their metabolism. Our results constitute a basis for the development of a new generation of optogenetic systems, which can be used either alone or in combination with blue-light

optogenetic tools. Since we used practically unmodified BphP1 and PpsR2 proteins, we expect that the light sensitivity, kinetics, and reversibility of their interaction may be amenable to further optimization using molecular engineering approaches.

METHODS

Methods and any associated references are available in the online version of the paper.

Accession codes. Data are deposited in the Genbank database with the following accession numbers: PpsR2, KX063612; BphP1, KX063613.

Note: Any Supplementary Information and Source Data files are available in the online version of the paper.

ACKNOWLEDGMENTS

We thank E. Giraud (Institute for Research and Development, Marseille), M. Papiz (Liverpool University), T. Beatty (University of British Columbia), W. Weber (University of Freiburg), P. Hackett (University of Minnesota), Z. Izsvak (Max Delbrück Center for Molecular Medicine), Y. Yang (East China University of Science and Technology), and S. Masuda (Tokyo Institute of Technology) for plasmids and D. Shcherbakova, K. Chernov, and T. Redchuk for useful suggestions. This work was sponsored by National Institutes of Health grants GM073913, GM108579, and CA164468 to V.V.V.

AUTHOR CONTRIBUTIONS

A.A.K. and A.A.S. characterized the proteins *in vitro*, in mammalian cell culture, and *in vivo*. V.V.V. planned and directed the project and, together with A.A.K. and A.A.S., designed the experiments, analyzed the data, and wrote the manuscript.

COMPETING FINANCIAL INTERESTS

The authors declare no competing financial interests.

1. Shcherbakova, D.M., Shemetov, A.A., Kaberniuk, A.A. & Verkhusha, V.V. Natural photoreceptors as a source of fluorescent proteins, biosensors, and optogenetic tools. *Annu. Rev. Biochem.* **84**, 519–550 (2015).
2. Motta-Mena, L.B. *et al.* An optogenetic gene expression system with rapid activation and deactivation kinetics. *Nat. Chem. Biol.* **10**, 196–202 (2014).
3. Kawano, F., Suzuki, H., Furuya, A. & Sato, M. Engineered pairs of distinct photoswitches for optogenetic control of cellular proteins. *Nat. Commun.* **6**, 6256 (2015).
4. Stierl, M. *et al.* Light modulation of cellular cAMP by a small bacterial photoactivated adenylyl cyclase, bPAC, of the soil bacterium Beggiatoa. *J. Biol. Chem.* **286**, 1181–1188 (2011).
5. Taslimi, A. *et al.* An optimized optogenetic clustering tool for probing protein interaction and function. *Nat. Commun.* **5**, 4925 (2014).
6. Lee, S. *et al.* Reversible protein inactivation by optogenetic trapping in cells. *Nat. Methods* **11**, 633–636 (2014).
7. Ni, M., Tepperman, J.M. & Quail, P.H. Binding of phytochrome B to its nuclear signalling partner PIF3 is reversibly induced by light. *Nature* **400**, 781–784 (1999).
8. Levskaya, A., Weiner, O.D., Lim, W.A. & Voigt, C.A. Spatiotemporal control of cell signalling using a light-switchable protein interaction. *Nature* **461**, 997–1001 (2009).
9. Gomez, E.J., Gerhardt, K., Judd, J., Tabor, J.J. & Suh, J. Light-activated nuclear translocation of adeno-associated virus nanoparticles using phytochrome B for enhanced, tunable, and spatially programmable gene delivery. *ACS Nano.* **10**, 225–237 (2016).
10. Weissleder, R. & Ntziachristos, V. Shedding light onto live molecular targets. *Nat. Med.* **9**, 123–128 (2003).
11. Ulijasz, A.T. & Vierstra, R.D. Phytochrome structure and photochemistry: recent advances toward a complete molecular picture. *Curr. Opin. Plant Biol.* **14**, 498–506 (2011).
12. Piatkevich, K.D., Subach, F.V. & Verkhusha, V.V. Engineering of bacterial phytochromes for near-infrared imaging, sensing, and light-control in mammals. *Chem. Soc. Rev.* **42**, 3441–3452 (2013).
13. Müller, K. *et al.* A red/far-red light-responsive bi-stable toggle switch to control gene expression in mammalian cells. *Nucleic Acids Res.* **41**, e77 (2013).
14. Tran, M.T. *et al. In vivo* image analysis using iRFP transgenic mice. *Exp. Anim.* **63**, 311–319 (2014).
15. Shcherbakova, D.M., Baloban, M. & Verkhusha, V.V. Near-infrared fluorescent proteins engineered from bacterial phytochromes. *Curr. Opin. Chem. Biol.* **27**, 52–63 (2015).
16. Shcherbakova, D.M. & Verkhusha, V.V. Near-infrared fluorescent proteins for multicolor *in vivo* imaging. *Nat. Methods* **10**, 751–754 (2013).
17. Shcherbakova, D.M. *et al.* Molecular basis of spectral diversity in near-infrared phytochrome-based fluorescent proteins. *Chem. Biol.* **22**, 1540–1551 (2015).
18. Piatkevich, K.D., Subach, F.V. & Verkhusha, V.V. Far-red light photoactivatable near-infrared fluorescent proteins engineered from a bacterial phytochrome. *Nat. Commun.* **4**, 2153 (2013).
19. Filonov, G.S. & Verkhusha, V.V. A near-infrared BiFC reporter for in vivo imaging of protein-protein interactions. *Chem. Biol.* **20**, 1078–1086 (2013).
20. Auldridge, M.E. & Forest, K.T. Bacterial phytochromes: more than meets the light. *Crit. Rev. Biochem. Mol. Biol.* **46**, 67–88 (2011).
21. Ryu, M.H. & Gomelsky, M. Near-infrared light responsive synthetic c-di-GMP module for optogenetic applications. *ACS Synth. Biol.* **3**, 802–810 (2014).
22. Ryu, M.H. *et al.* Engineering adenylate cyclases regulated by near-infrared window light. *Proc. Natl. Acad. Sci. USA* **111**, 10167–10172 (2014).
23. Gasser, C. *et al.* Engineering of a red-light-activated human cAMP/cGMP-specific phosphodiesterase. *Proc. Natl. Acad. Sci. USA* **111**, 8803–8808 (2014).
24. Wagner, J.R., Zhang, J., Brunzelle, J.S., Vierstra, R.D. & Forest, K.T. High resolution structure of Deinococcus bacteriophytochrome yields new insights into phytochrome architecture and evolution. *J. Biol. Chem.* **282**, 12298–12309 (2007).
25. Rockwell, N.C. & Lagarias, J.C. A brief history of phytochromes. *ChemPhysChem* **11**, 1172–1180 (2010).
26. Rottwinkel, G., Oberpichler, I. & Lamparter, T. Bathy phytochromes in rhizobial soil bacteria. *J. Bacteriol.* **192**, 5124–5133 (2010).
27. Kojadinovic, M. *et al.* Dual role for a bacteriophytochrome in the bioenergetic control of *Rhodopseudomonas palustris*: enhancement of photosystem synthesis and limitation of respiration. *Biochim. Biophys. Acta* **1777**, 163–172 (2008).
28. Bellini, D. & Papiz, M.Z. Structure of a bacteriophytochrome and light-stimulated protomer swapping with a gene repressor. *Structure* **20**, 1436–1446 (2012).
29. Hussain, N.K. *et al.* Endocytic protein intersectin-l regulates actin assembly via Cdc42 and N-WASP. *Nat. Cell Biol.* **3**, 927–932 (2001).
30. Hall, A. Rho GTPases and the actin cytoskeleton. *Science* **279**, 509–514 (1998).
31. Nobes, C.D. & Hall, A. Rho, rac, and cdc42 GTPases regulate the assembly of multimolecular focal complexes associated with actin stress fibers, lamellipodia, and filopodia. *Cell* **81**, 53–62 (1995).
32. Orth, P., Schnappinger, D., Hillen, W., Saenger, W. & Hinrichs, W. Structural basis of gene regulation by the tetracycline inducible Tet repressor-operator system. *Nat. Struct. Biol.* **7**, 215–219 (2000).
33. Wang, X., Chen, X. & Yang, Y. Spatiotemporal control of gene expression by a light-switchable transgene system. *Nat. Methods* **9**, 266–269 (2012).
34. Chen, X., Li, T., Wang, X. & Yang, Y. A light-switchable bidirectional expression module allowing simultaneous regulation of multiple genes. *Biochem. Biophys. Res. Commun.* **465**, 769–776 (2015).
35. Schönig, K., Bujard, H. & Gossen, M. The power of reversibility regulating gene activities via tetracycline-controlled transcription. *Methods Enzymol.* **477**, 429–453 (2010).
36. Albanese, C., Hulit, J., Sakamaki, T. & Pestell, R.G. Recent advances in inducible expression in transgenic mice. *Semin. Cell Dev. Biol.* **13**, 129–141 (2002).
37. Toettcher, J.E., Weiner, O.D. & Lim, W.A. Using optogenetics to interrogate the dynamic control of signal transmission by the Ras/Erk module. *Cell* **155**, 1422–1434 (2013).
38. Müller, K. *et al.* Synthesis of phycocyanobilin in mammalian cells. *Chem. Commun. (Camb.)* **49**, 8970–8972 (2013).
39. International Electrotechnical Commission. *Safety of Laser Products–Part 1: Equipment Classification and Requirements* 3rd edn. (International Electrotechnical Commission, 2014).

ONLINE METHODS

Design of bacterial and mammalian plasmids. An *RpBphP1* gene of *R. palustris* (NCBI Gene *rpa1537*) was kindly provided by E. Giraud (Institute for Research and Development, France). An *RpPpsR2* gene of *R. palustris* (NCBI Gene *rpa1536*) was kindly provided by M. Papiz (Liverpool University, UK) and T. Beatty (University of British Columbia, Canada). A DHPH domain of human intersectin 1 was PCR amplified from a pAL189 plasmid (Addgene #22278)[8]. An *mRuby2* gene was PCR amplified from a pcDNA3–mRuby2 plasmid (Addgene #40260)[40]. A transactivation domain of transactivating tegument protein VP16 from *Herpes simplex* was PCR amplified from a pGV–2ER plasmid (Systasy). An *Rluc8* gene encoding modified luciferase from *Renilla reniformis* was PCR amplified from a Nano-lantern/pcDNA3 plasmid (Addgene #51970). A *SEAP* gene was PCR amplified from a pKM611 plasmid kindly provided by W. Weber (University of Freiburg, Germany). A plasmid pKM022 encoding PhyB (1-650) was obtained by mutagenesis, using the pKM020 plasmid as a template[13]. A *TetR* gene (residues 1–207) that binds DNA in the absence of tetracycline/doxycycline was PCR amplified from a pTet-Off vector (Clontech).

The reporter plasmids pTRE–Tight–EGFP, pTRE–Tight–SEAP, and pTRE–Tight–Rluc8 were obtained by cloning the *EGFP*, *SEAP*, and *Rluc8* genes, respectively, into a pTRE–Tight2 vector (Addgene #19407). The LightON system plasmids, pGAVPO (encoding GAL4(65)-VVD-p65 activation domain) and pU5–mCherry, were kindly provided by Y. Yang (East China University of Science and Technology, China)[33]. A pU5–Rluc8 reporter plasmid was generated by substitution of an mCherry gene in the pU5–mCherry plasmid with the *Rluc8* gene. To develop stable preclonal cell mixtures of HeLa cells, plasmids encoding a transposase SB100X, pCMV(CAT)T7-SB100 (Addgene #34879), and transposon-bearing plasmids pT2/SVNeo and pT2/BH (Addgene #26553 and #26556)[41] were used. An IRESv10 with ~3-fold reduced expression strength[42] was obtained from IRES using mutagenesis.

For bacterial expression of the BphP1, BphP1-mRuby2, and PpsR2-mRuby2 proteins, vectors pBAD/His-D, pBAD/His-B (Life Technologies-Invitrogen), and pET22b (Novagen) were used, respectively. In the pET22b vector, an N-terminal pelB signal was replaced with a Strep-tag II.

Mammalian expression plasmids were based on either a pEGFP-N1 vector (Clontech), with either a standard CMV promoter or its truncated CMVd1 form, or on a pFC15K vector (Promega) with the truncated CMVd1 promoter. The flexible linkers of 10 (-D-S-A-G-S-A-G-S-A-G-), 16 (-S-A-G-G-S-A-G-G-S-A-G-G-S-A-G-G-), 20 (-S-A-G-G-S-A-G-G-S-A-G-G-S-A-G-G-S-A-G-G-), or 24 (-S-G-G-G-S-G-G-G-S-G-G-G-S-G-G-G-S-G-G-G-S-G-G-G-) amino acids, a C-terminal membrane-localization CAAX signal from Kras4B (-K-K-K-K-K-K-S-K-T-K-C-V-I-M), a nuclear localization signal of nuclear cap-binding protein subunit 1 (MS-R-R-R-H-S-Y-E-N-D-G-G-Q-P-H-K-R-R-K-), and a Strep-tag II (-W-S-H-P-Q-F-E-K-) were added by oligonucleotide annealing. The designed plasmids are summarized in **Supplementary Table 2**.

Protein expression and purification. BphP1 and BphP1-mRuby2 proteins with polyhistidine tags on the N terminus were expressed in LMG194 bacterial cells (Life Technologies-Invitrogen) containing a pWA23h plasmid encoding heme oxygenase for biliverdin synthesis in *Escherichia coli*[18]. The bacterial cells were grown in RM medium supplemented with ampicillin, kanamycin, and 0.02% rhamnose for 6–8 h, followed by an induction of the protein expression by adding 0.002% arabinose. The proteins were purified using an Ni-NTA agarose (Qiagen). The PpsR2 and PpsR2-mVenus proteins with a Strep-tag II at the N terminus and a polyhistidine tag at the C terminus were expressed in BL21(DE3) bacterial cells grown in LB medium supplemented with ampicillin for 6 h, followed by an induction of a protein expression with 250 μM IPTG. The proteins were first purified with an Ni-NTA agarose (Qiagen) followed by purification with a Strep-Tactin sepharose (IBA Lifesciences).

***In vitro* characterizations of BphP1 properties.** For absorbance measurements, a Hitachi U-2000 spectrophotometer was used. For fluorescence measurements of mRuby2 fusions, a FluoroMax-3 spectrofluorometer (Horiba-Jobin Yvon) was equipped with a 600-nm shortpass filter before detector was used. A photoconversion of BphP1 containing proteins was performed with 740/25-nm and 636/20-nm custom-assembled LED sources in quartz microcuvettes (Starna Cells). A determination of action spectrum was performed by measurement of the change in absorbance of Pfr-state BphP1 at 780 nm upon illumination with photoconversion light. The FluoroMax-3 spectrofluorometer was used as a light source. The illumination time was normalized to total amount of irradiated light energy, measured with a PM100 optical powermeter equipped with a S130A sensor (ThorLabs) at the respective wavelength. A half-time of Pr→Pfr transition (or dark relaxation) was measured by registering of absorbance at 780 nm after 5 min illumination of samples with 740/25 nm. Samples containing fixed quantities of BphP1 (5 μM) and various quantities of PpsR2 (0–5 μM) were preincubated in darkness for 30 min. Reversible dark relaxation cycles were obtained by the registration of 780-nm absorbance of protein mixture at BphP1:PpsR2 molar ratio of 8:1. To study changes in mRuby2 fluorescence due to FRET between the PpsR2-mRuby2 fusion and the Pr state of BphP1, the proteins (2.5 μM each) were preincubated in darkness for 30 min and then transferred to a microcuvette. An mRuby2 fluorescence intensity was registered every 30 s with excitation 545/2 nm and emission 585/10 nm. All spectroscopic measurements were performed at room temperature in PBS.

Mammalian cell culture. HeLa cells were purchased from the ATCC (CCL-2 line) and were not additionally authenticated or tested for mycoplasma contamination. The cells were grown in DMEM medium supplemented with 10% FBS, penicillin–streptomycin mixture, and 2 mM glutamine (all from Life Technologies-Invitrogen) at 37 °C. For imaging, 10^5 cells were plated on 35-mm glass-bottom culture dishes (MatTek) precoated with ECL mixture (EMD-Millipore). Transient cell transfections were performed using an Effectene Transfection Reagent (Qiagen).

Preclonal mixtures of HeLa cells were obtained using the plasmid-based Sleeping Beauty transposon system. For this, sequences desired for genome integration were cloned into the transposon-bearing plasmids pT2/BH or pT2/SVNeo and cotransfected with a plasmid encoding a hyperactive transposase SB100X. Cells were further selected with 700 μg/ml of G418 antibiotic for two weeks and enriched using a FACSAria sorter (BD Biosciences), resulting in the preclonal HeLa cell mixtures stably expressing BphP1-mCherry-TetR.

doi:10.1038/nmeth.3864

For light-induced relocalization to plasma membrane, HeLa cells were transiently cotransfected with pKA-140 or pKA-142 and pKA-141 plasmids in 1:1 ratio. For light-induced cytoskeletal rearrangement, cells were cotransfected with pKA-142 (or pKA-147) and pKA-144 plasmids in 1:2 ratio. The cell light activation and imaging were typically performed 48 h after the transfection. For light-induced nuclear relocalization, HeLa cells stably expressing BphP1-mCherry-TetR were transiently transfected with pCMV-160. To study light-induced transcription activation in the TetR-based system, HeLa cells stably expressing BphP1-mCherry-TetR were cotransfected with pCMV-104 and pTRE–Tight–EGFP, pTRE–Tight–SEAP or pTRE–Tight–Rluc8 plasmids in 5:1 ratio. To compare the PhyB–PIF6 system with the BphP1–PpsR2 system, HeLa cells were transfected with pKM022 and pTRE–Tight–SEAP plasmids in 2:1 ratio. All procedures after the transfection were performed as described in the PhyB–PIF6 paper[13].

Cell light activation and imaging. Imaging was performed using an Olympus IX81 inverted epifluorescence microscope equipped with a 200-W metal halide arc lamp (Lumen 220PRO, Prior) and a 60×, 1.35 NA oil immersion objective lens (UPlanSApo, Olympus). During imaging HeLa cells were incubated in a cell imaging medium (Life Technologies-Invitrogen) and kept at 37 °C. Yellow (523/20-nm exciter and 565/40-nm emitter) and red (570/30-nm exciter and 615/30-nm emitter) channel filter sets (Chroma) were used for detection of mVenus and mCherry fluorescence, respectively. The Pfr→Pr photoconversion of BphP1 was done by illumination with 740/40-nm filters (Chroma).

For Pfr→Pr relocalization assay, HeLa cells were exposed to 740/40 nm and imaged every 15 s for 3 min. Intensity of activation light was 0.9 mW cm^{-2}. To quantify mCherry fluorescence in cell cytoplasm during BphP1 dark relaxation, HeLa cells were imaged every 3 min for 24 min, starting immediately after the Pfr→Pr photoconversion. Intensity profile of mCherry fluorescence through cell was determined using ImageJ v.1.46f software. Intensity of mCherry fluorescence in cytoplasm and nucleus was measured using SlideBook v.4.2.09.

To study light-induced cytoskeletal rearrangements, the Pfr→Pr photoconversion was done by illuminating cells using 740/40-nm filters for 3 min and imaging these cells every 15 s, followed by maintaining BphP1 in the Pr state by illuminating BphP1 with 740/40 nm for 15 s every minute and imaging BphP1 every 60 s. The intensity of activation light was 0.2 mW cm^{-2}. The total time of cell imaging was 30 min. The light power densities were measured at a back focal plane of a 60×, 1.35 NA objective lens. Membrane-localized mVenus was used for determination of cell area. The data were analyzed using ImageJ v.1.46f software.

Unless otherwise indicated, a light-induced transcription activation of HeLa cells was performed with a 740/25-nm LED source at 1.0 mW cm^{-2} using the 30 s On and 180 s Off cycle in a CO_2 incubator at 37 °C. Time of illumination varied in different experiments. For nuclear localization and EGFP or SEAP transcription activation experiments, cells were illuminated for 24 and 48 h, respectively. For kinetic studies of SEAP accumulation in culture media, three different illumination regimes were used: 72 h of 740/25 nm; 12 h of 740/25 nm followed by 60 h of darkness; and 12 h of 740/25 nm followed by 12 h of 636/20 nm followed by 38 h of darkness. To measure light sensitivity of SEAP expression activation, HeLa cells were irradiated with either 740/25-nm (with BphP1–PpsR2) or 660/20-nm (with PhyB–PIF6) light of various power densities (5–1000 μW cm^{-2}). Light power densities and illumination durations were converted to photon counts.

Light-induced LightON transcription activation of *Rluc8* in HeLa cells was performed as described in the original paper[33]. In brief, HeLa cells were transfected with pGAVPO and pU5–Rluc8 plasmids in 1:1 ratio. Then, cells were kept in darkness for 10 h. After change of culture medium, the cells were continuously illuminated with a 470/15-nm LED array (LuxeonStar) of 1 mW cm^{-2}, or the cells remained in darkness for 48 h before analysis. For analysis, the cells were resuspended in PBS and disrupted by freezing–thawing. An Rluc8 bioluminescence signal was measured in supernatants after the addition of 5 μM coelenterazine h (NanoLight Technology). A signal was detected using an IVIS Spectrum instrument (PerkinElmer/Caliper Life Sciences) and analyzed using Living Image 3.0 software (PerkinElmer/Caliper Life Sciences).

Flow cytometry analysis. Flow cytometry analysis of light-induced EGFP expression was performed 48 h after the HeLa cell transfection using a LSRII flow cytometer (BD Biosciences) equipped with a 488-nm laser and a 530/40-nm emission filter and with a 561-nm laser and 610/20-nm emission filter. To calculate an efficiency of the light-induced EGFP expression, a mean fluorescent intensity of EGFP-positive cells was multiplied by the number of positive cells, resulting in the total amount of synthesized proteins. Gates for counting EGFP-positive cells were set using nontransfected cells as a negative control. Typically, the cell samples were triplicated. Minimally, 5×10^4 cells were analyzed per sample. The data were analyzed using FACSDiva v. 6.1.3 and FlowJo v. 7.6.2 software.

Secreted alkaline phosphatase assay. For SEAP detection in culture media, a Great EscApe fluorescent SEAP Assay kit (Clontech) was used. 25-μl aliquots of cell culture media from wells of a 12-well plate were collected at each time point and stored at −20 °C. For kinetics studies, a culture medium was changed with a fresh medium at each time point. Fluorescence intensity of the SEAP reaction product was measured using the SpectraMax-M2 plate reader (Molecular Devices).

Light activation and imaging in mice. 2- to 3-month-old female FVB mice (National Cancer Institute, NIH) of 20–25 g body weight were used for *in vivo* comparison of the LightON and BphP1–PpsR2 systems. To compare the efficiency of the light-induced transcription activation, HeLa cells with either the LightON system or the BphP1–PpsR2 system were injected subcutaneously in the interscapular area of FVB mice. For better illumination, the fur on the backs of the mice was removed using a depilatory cream. For the LightON system, HeLa cells were cotransfected with the pGAVPO and pU5–Rluc8 plasmids in a 1:1 ratio; and for the BphP1–PpsR2 system, HeLa cells stably expressing BphP1-mCherry-TetR were cotransfected with the plasmid encoding NLS-PpsR2-VP16 and the pTRE–Tight–Rluc8 reporter plasmid in a 5:1 ratio. For both systems, the 3×10^6 HeLa cells in 100 μl of RPMI-1640 media supplemented with 2 mM L-glutamine were injected subcutaneously 24 h after the transfection. All manipulations with cells before and during the injection

were performed under a 640-nm safelight for the LightON system and under a 530-nm safelight for the BphP1–PpsR2 system. After injection, mice were placed in transparent cages illuminated from the top with either the 470/15-nm LED array or the 740/25-nm LED array for the LightON and BphP1–PpsR2 systems, respectively. Intensities of 470/15-nm light and 740/25-nm light were the same and equal to 1 mW cm^{-2}. After injection, control mice were kept in darkness in conventional cages. Animals were either continuously illuminated or kept in darkness for 48 h, and they were released every 12 h and fed for 30 min. Each experimental group contained three mice.

For hydrodynamic transfection into liver[43], the Swiss Webster 2- to 3-month-old female mice (National Cancer Institute, NIH) with body weights of 22–25 g were used. For the BphP1–PpsR2 system, 50 μg of the pKA–207I10 plasmid and 5 μg of the pTRE–Tight–Rluc8 reporter plasmid in 2.5 ml of PBS were intravenously injected through a tail vein. For hydrodynamic transfection by the LightON system, we used the plasmid amounts either indicated in the original paper[33] (10 μg of the pGAVPO plasmid and 300 μg of the pU5–Rluc8 plasmid) or similar to those used for the BphP1–PpsR2 system (50 μg of the pGAVPO plasmid and 5 μg of the pU5–Rluc8 plasmid). The mice were placed in transparent cages and illuminated from the bottom with either the 470/15-nm LED array or the 740/25-nm LED array for the LightON and the BphP1–PpsR2 systems, respectively. Intensity of the activation light was the same and equal to 5 mW cm^{-2}. For better illumination and imaging, the belly fur was removed using a depilatory cream. Control animals were kept in conventional cages in complete darkness. Animals were continuously illuminated or kept in darkness for 72 h, and every 12 h they were released and fed for 30 min. Each experimental group contained three mice.

For bioluminescence detection, either 48 h after the HeLa cells injection or every 24 h after the hydrodynamic transfection of livers the animals were imaged using an IVIS Spectrum instrument (PerkinElmer/Caliper Life Sciences) in luminescence mode with an open emission filter. Throughout the imaging, animals were maintained under anesthesia with 1.5% vaporized isoflurane. Prior to imaging, 80 μg of Inject-A-Lume coelenterazine substrate for Rluc8 (NanoLight Technology) was intravenously injected through a retro-orbital vein. Data were analyzed using Living Image 3.0 software (Perkin Elmer/Caliper Life Sciences).

All animal experiments were performed in an AAALAC-approved facility using protocols approved by the Albert Einstein College of Medicine Animal Usage Committee. 30 mice were used in this study.

40. Lam, A.J. *et al.* Improving FRET dynamic range with bright green and red fluorescent proteins. *Nat. Methods* **9**, 1005–1012 (2012).
41. Cui, Z., Geurts, A.M., Liu, G., Kaufman, C.D. & Hackett, P.B. Structure-function analysis of the inverted terminal repeats of the sleeping beauty transposon. *J. Mol. Biol.* **318**, 1221–1235 (2002).
42. Koh, E.Y. *et al.* An internal ribosome entry site (IRES) mutant library for tuning expression level of multiple genes in mammalian cells. *PLoS ONE* **8**, e82100 (2013).
43. Liu, F., Song, Y. & Liu, D. Hydrodynamics-based transfection in animals by systemic administration of plasmid DNA. *Gene Ther.* **6**, 1258–1266 (1999).

doi:10.1038/nmeth.3864

Supplementary Table 1.

Characteristics of BphP1 and its interaction with PpsR2 *in vitro*.

Proteins	Chromo-phore state	Absorbance maximum, nm	Extinction coefficient[1], $M^{-1}cm^{-1}$	Absorbance change upon photoconversion, fold[2]		Half-time (s) of[3]	
				at 756 nm	at 678 nm	photoconversion	dark relaxation
BphP1	Pr	678	87,500	4.3 (7.0)	0.48 (0.45)	16 (Pr→Pfr, with 636/20 nm)	210
BphP1 and PpsR2						30 (Pr→Pfr, with 636/20 nm)	900
BphP1	Pfr	756	78,300			19 (Pfr→Pr, with 740/25 nm)	N.A.
BphP1 and PpsR2						60 (Pfr→Pr, with 740/25 nm)	

[1]Calculated based on an extinction coefficient of BV, as described[1]; [2]Measured after irradiation either by a 740/25 nm LED array or by a 785/2 nm laser diode (in parenthesis); [3]BphP1:PpsR2 molar ratio of 8:1 and photoconversion light intensity of 2 mW cm^{-2} were used. N.A., not applicable.

Nature Methods: doi:10.1038/nmeth.3864

Supplementary Table 2.

Bacterial and mammalian plasmids designed in this paper.

Plasmid	Figure	Vector backbone	Promoter	Insert
pKA-100	1, S1-S3	pBAD/His-D	PBAD	*Bgl*II-BphP1-*Eco*RI
pKA-101	S2	pBAD/His-B	PBAD	*Bgl*II-BphP1-*Eco*RI-10aaLinker-*Spe*I-mRuby2-*Hind*III
pKA-138.2	1, S2	pET-22b	T7	*Nde*I-Strep-tag II-*Nco*I-PpsR2-*Hind*III-20aaLinker-*Age*I-mRuby2-*Xho*I-His-tag
pKA-140	2	pEGFP-N1	CMV	*Kpn*I-PpsR2(C439S)-*Hind*III-20aaLinker-*Age*I-mVenus-*Nhe*I-Kras4BCT-*Not*I
pKA-141	2, S4	pFC15K	CMVd1	*Nhe*I-BphP1-*Eco*RI-10aaLinker-*Spe*I-mCherry-*Xba*I
pKA-142	2, 3, S4, S5	pFC15K	CMVd1	*Asi*SI-PpsR2(C439S)-*Hind*III-20aaLinker-*Age*I-mVenus-*Nhe*I-Kras4BCT-*Not*I
pKA-144	3, S5	pFC15K	CMVd1	*Nhe*I-BphP1-*Eco*RI-10aaLinker-*Spe*I-mCherry-*Bsr*GI-20aaLinker-*Xba*I-IntersectinDHPH-*Not*I
pKA-147	3	pFC15K	CMVd1	*Asi*SI-mVenus-*Nhe*I-Kras4BCT-*Not*I
pCMV-160	4, S6	pEGFP-N1	CMV	*Asi*SI-NLS-*Age*I-PpsR2(C439S)-*Hind*III-20aaLinker-*Age*I-mVenus-*Xba*I
pT2/SVNeo-103	4, 5, S6-10, S13	pT2/SVNeo	CMVd1	IRDR-CMVd1- *NheI*-BphP1-*EcoRI*-10aaLinker-*SpeI*-mCherry-*BsrGI*-24aaLinker-*XbaI*-TetR-*NotI*-NeoR-IRDR
pKA-207I10	5	pIRES-EGFP	CMV	*NheI*-NLS-*AgeI*-PpsR2-*HindIII*-20aaLinker-*NcoI*-VP16-*BglII*-IRESv10-*NcoI*-BphP1-*EcoRI*-10aaLinker-mCherry-TetR-*NotI*
pCMV-104	4, 5, S7-10, S13	pEGFP-N1	CMV	*Asi*SI-NLS-*Age*I-PpsR2(C439S)-*Hind*III-20aaLinker-*Age*I-VP16-*Xba*I
pTRE-Tight-SEAP	4, S7, S8, S10	pTRE-Tight2	CMV_{min}	*Xho*I-7x*tet-responsive element*-P_{minCMV}-*Bam*HI-SEAP-*Not*I
pTRE-Tight-EGFP	S9	pTRE-Tight2	CMV_{min}	*Xho*I-7x*tet-responsive element*-P_{minCMV}-*BamHI*-EGFP-*Not*I
pTRE-Tight-Rluc8	5, S14	pTRE-Tight2	CMV_{min}	*Xho*I-7x*tet-responsive element*-P_{minCMV}-*BamHI*-Rluc8-*Not*I
pU5-Rluc8	5, S13-15	pU5-mCherry	min TATA-box promoter	5x*GAL4-binding UAS-minimal promoter*-*Hind*III- Rluc8-*Bam*HI

Supplementary Figure 1.

Kinetics of BphP1 photoconversion *in vitro*.

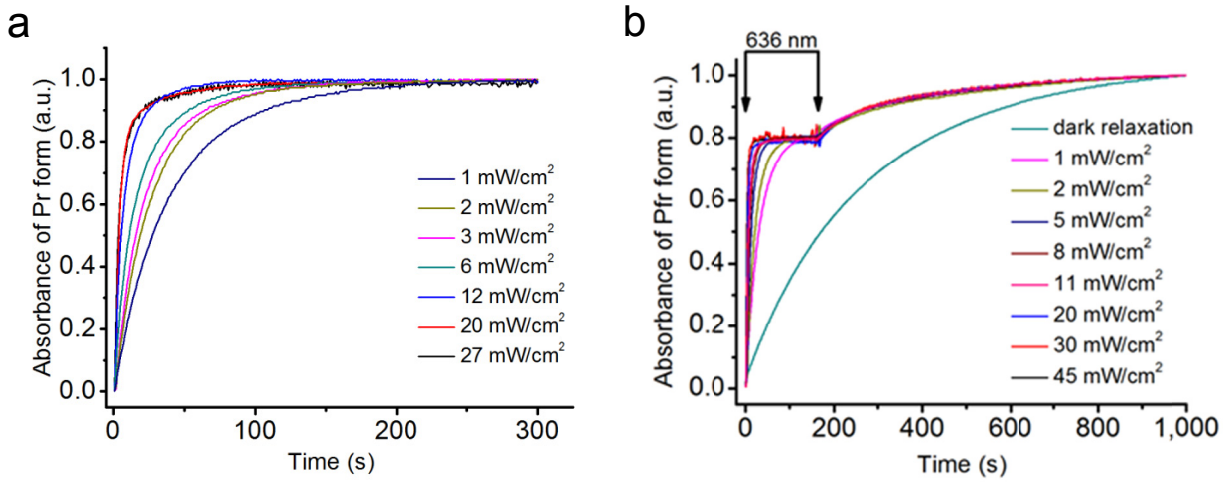

(**a**) Dependence of the Pfr→Pr photoconversion on the 740/25 nm light intensity. The gradual increase in absorbance of the Pr state was observed for all tested light intensities. Kinetic curves can be fitted with monoexponential functions ($R^2 \geq 0.958$ for all curves). (**b**) Dependence of the Pr→Pfr photoconversion on the 636/20 nm light intensity. The achievable with 636 nm light 0.8 value of the Pfr ground state is likely represents an equilibrium between the Pfr and Pr states because 636/20 light is also absorbed by the Pfr state, thus causing its partial photoconversion back to the Pr state.

Nature Methods: doi:10.1038/nmeth.3864

Supplementary Figure 2.

FRET-based approach for characterization of BphP1-PpsR2 interaction.

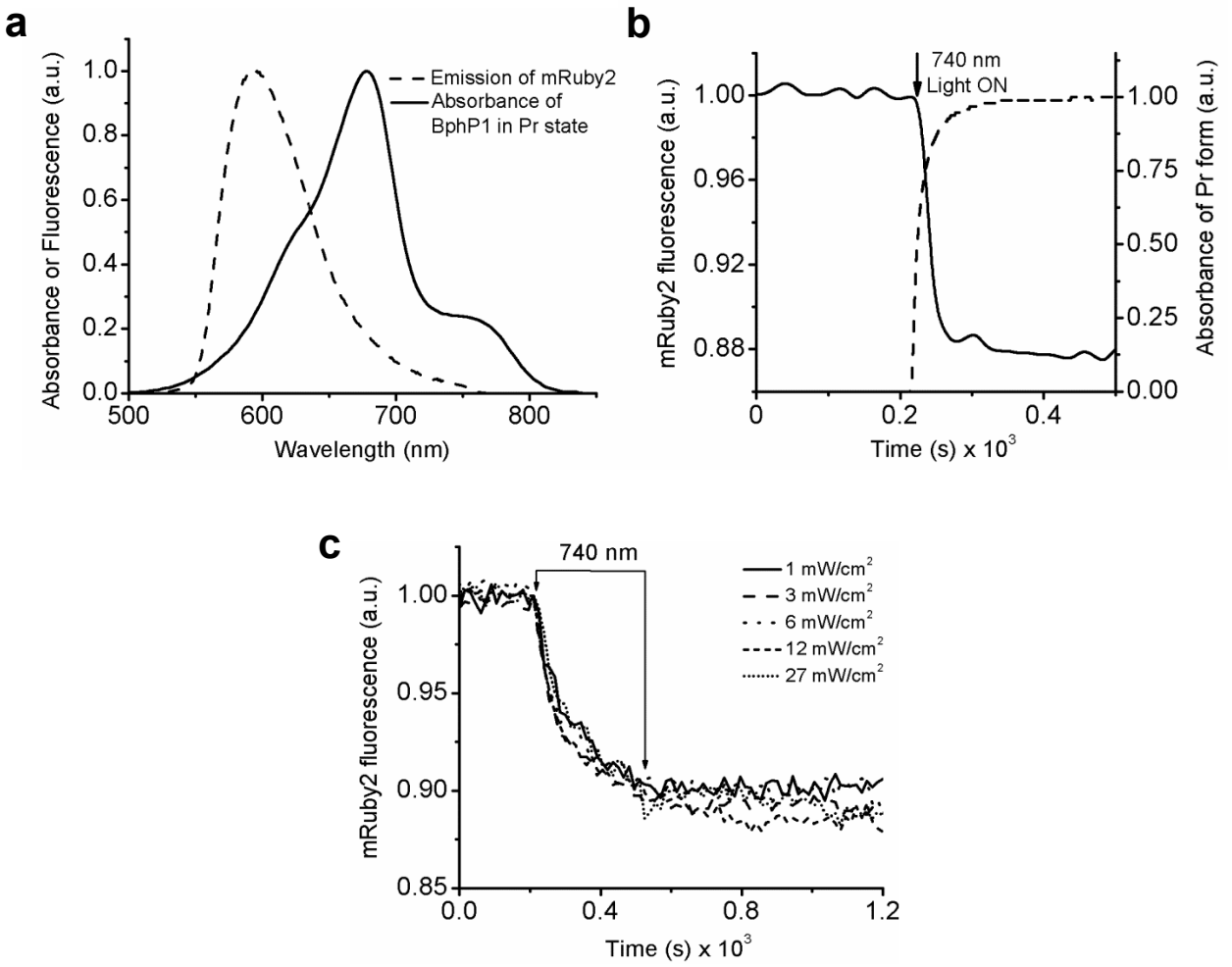

(**a**) Overlap of the emission spectrum of mRuby2 (dashed lines) and absorbance spectrum of BphP1 in the Pr state. (**b**) Changes of FRET (solid line) during Pfr→Pr photoconversion of BphP1-mRuby2 (dashed line). (**c**) Dependence of the FRET changes on power of 740/25 nm illumination of the PpsR2-mRuby2 and BphP1 mixture.

Supplementary Figure 3.

Overlap of wavelengths used for mVenus and mCherry excitation with action spectrum of Pfr→Pr photoconversion.

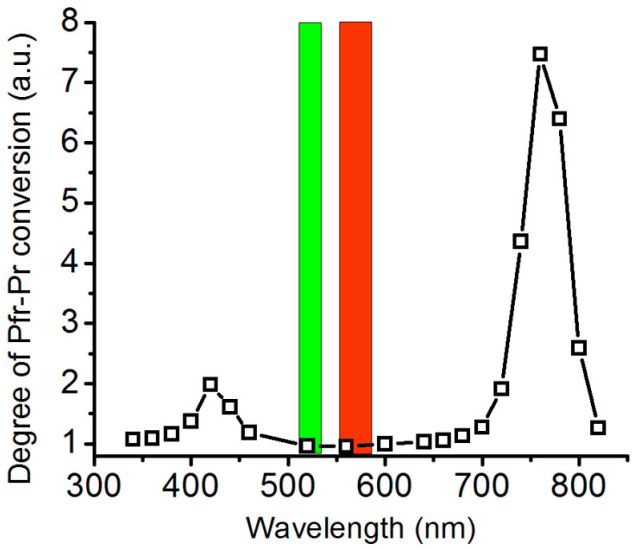

The green box outlines the wavelength range transmitted by 523/20 nm filter used for mVenus excitation, and the red box outlines the wavelength range transmitted by 570/30 nm filter used for mCherry excitation. The action spectrum of the Pfr→Pr photoconversion was measured as the relative decrease of Pfr absorbance detected at 780 nm upon irradiation with light of specific wavelength (open squares).

Nature Methods: doi:10.1038/nmeth.3864

Supplementary Figure 4.

Initial recovery of the mCherry cytoplasmic intensity under 650 nm light and in darkness.

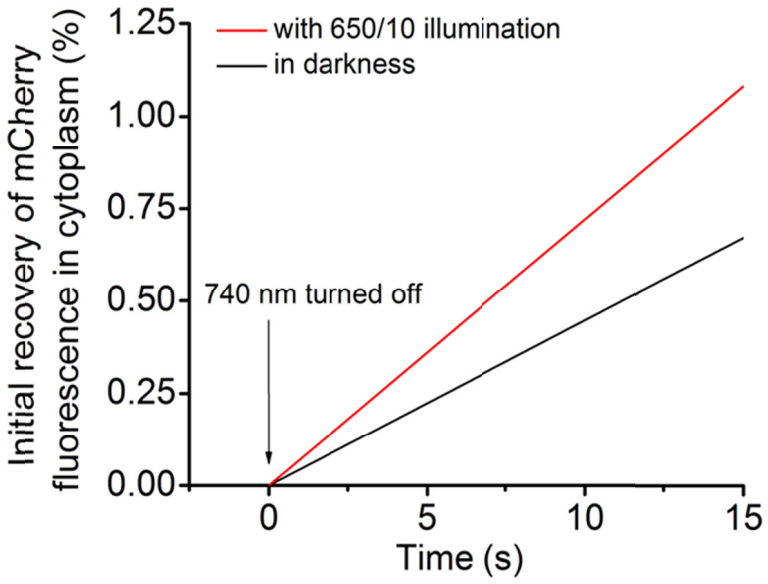

The linear fitting of the mean recovery kinetics of mCherry fluorescence in cytoplasm of cells right after 740/40 nm illumination either in darkness (black line; n=5) or after turning on 650/10 nm light (red line; n=5). The HeLa cells were co-expressing BphP1-mCherry and PpsR2-mVenus-CAAX constructs. The tangent of the angles that correspond to the initial mCherry recovery rates, are 0.044 % s^{-1} and 0.072 % s^{-1}, respectively.

Supplementary Figure 5.

Relative changes of the mCherry cytoplasmic intensity and the cell area.

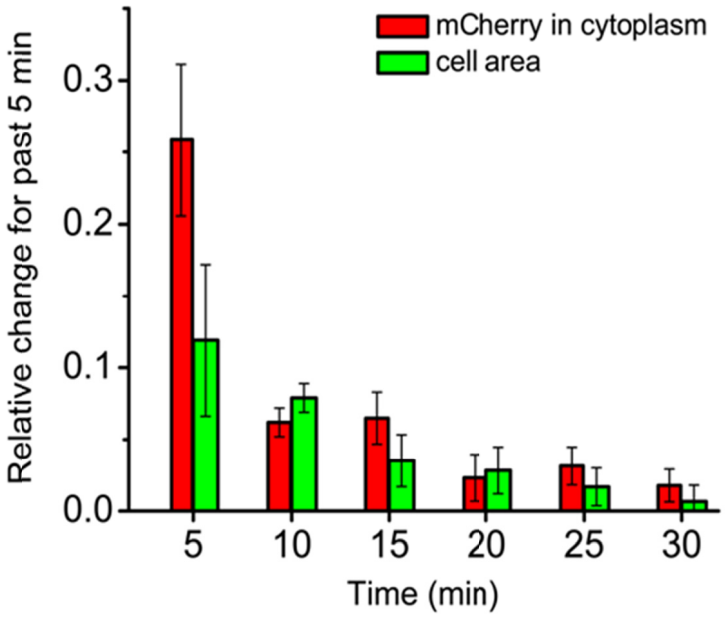

The relative decrease in mCherry cytoplasmic fluorescence and relative increase in cell area in 5 min periods from the beginning of cell illumination with 740/40 nm. The HeLa cells co-expressed the BphP1-mCherry-DHPH and PpsR2-mVenus-CAAX constructs (n=5, error bars are s.e.m.). The initial (during the first 5 min) relative decrease in the BphP1-mCherry-DHPH in cytoplasm was more than 2-fold larger than that of the increase in the cell area. No substantial difference between these two characteristics was observed in the later time periods.

Supplementary Figure 6.

Analysis of light-induced recruitment of BphP1-mCherry to nucleus.

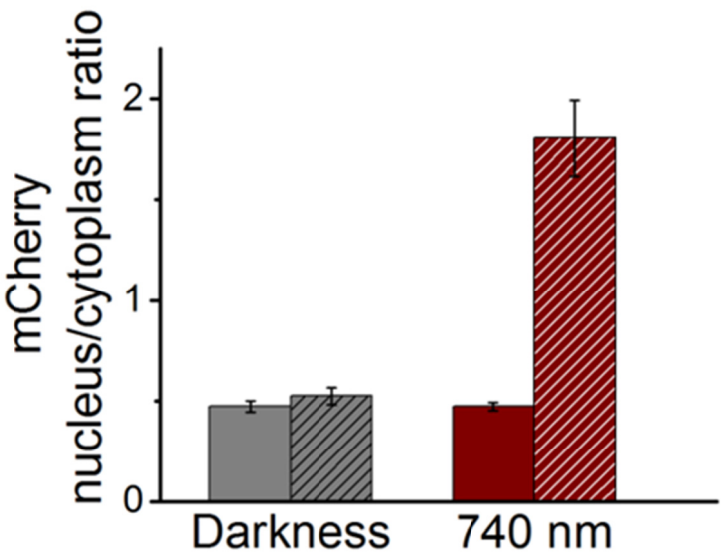

mCherry nucleus-to-cytoplasm intensity ratio in HeLa cells stably expressing BphP1-mCherry transfected with pCMV-160 (dashed bars) or not transfected (solid bars). Cells were kept in darkness or irradiated with 740/25 nm light (30 s On, 180 s Off) of 1 mW cm^{-2} for 24 h (n=20, error bars are s.e.m.). Cell imaging was performed using an epifluorescence microscope at 37^{o}C.

Supplementary Figure 7.

Characterization of light-inducible activation of SEAP expression using the TetR-*tetO* system.

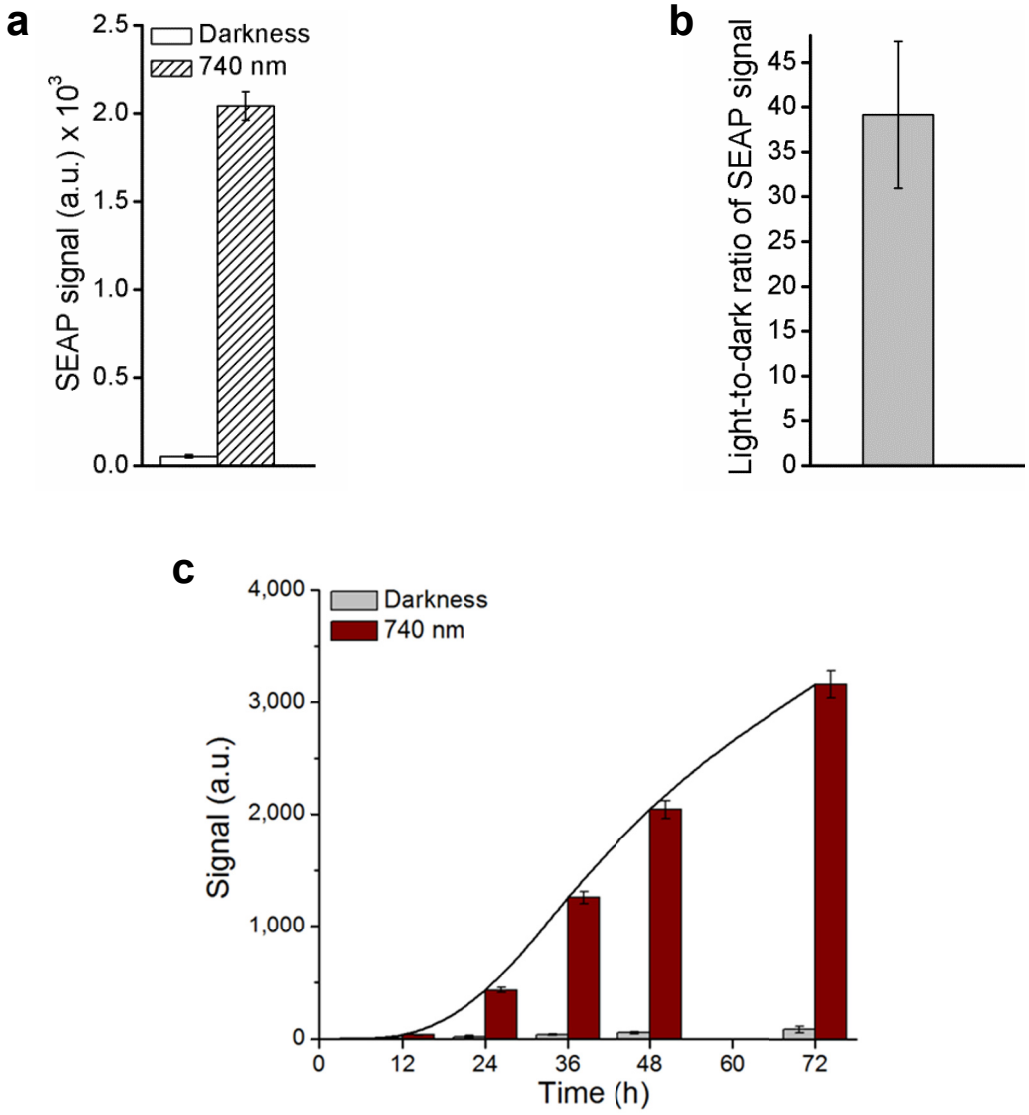

(**a**) SEAP signal detected in culture media of HeLa cells bearing BphP1-mCherry-TetR co-transfected with pCMV-104 and pTRE-Tight-SEAP (7×*tetO*) reporter plasmid after 48 h in darkness or under 740/25 nm light (n=3; error bars are s.e.m.). (**b**) Light-to-dark ratio of the SEAP signal shown in (a). (**c**) The kinetics of SEAP accumulation in culture media of illuminated with 740/25 nm light (dark red) and dark-treated (gray) HeLa cells stably expressing BphP1-mCherry-TetR, transiently co-transfected with pTRE-Tight-SEAP and pCMV-104 plasmids with a plasmids ratio of 1:5 (n=3, error bars are s.e.m.).

Nature Methods: doi:10.1038/nmeth.3864

Supplementary Figure 8.

Dependence of light-induced SEAP expression level on the power of 740 nm light.

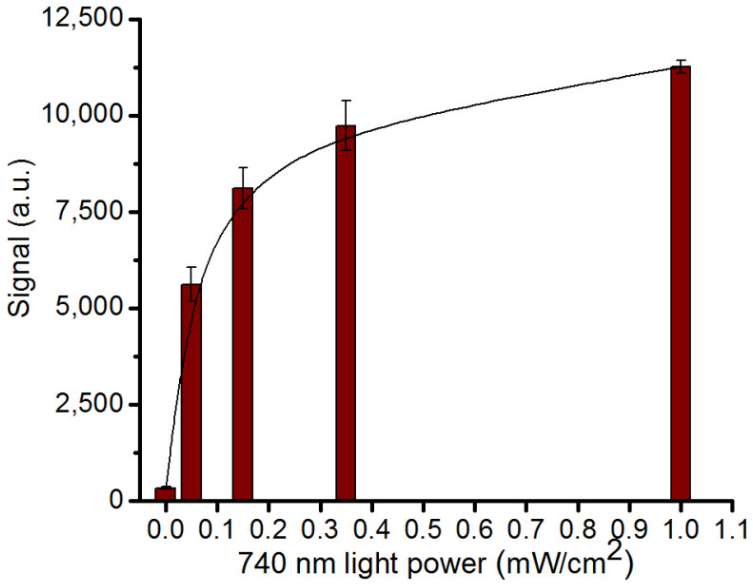

The light-induced expression of SEAP from the pTRE-Tight-SEAP reporter plasmid. SEAP signal was detected in HeLa cells with BphP1-mCherry-TetR, pTRE-Tight-SEAP and pCMV-104 plasmids. Cells were kept in darkness or under 740/25 nm light at different intensities (n=3, error bars are s.e.m.).

Supplementary Figure 9.

Light-induced expression of EGFP from the pTRE-Tight-EGFP reporter plasmid.

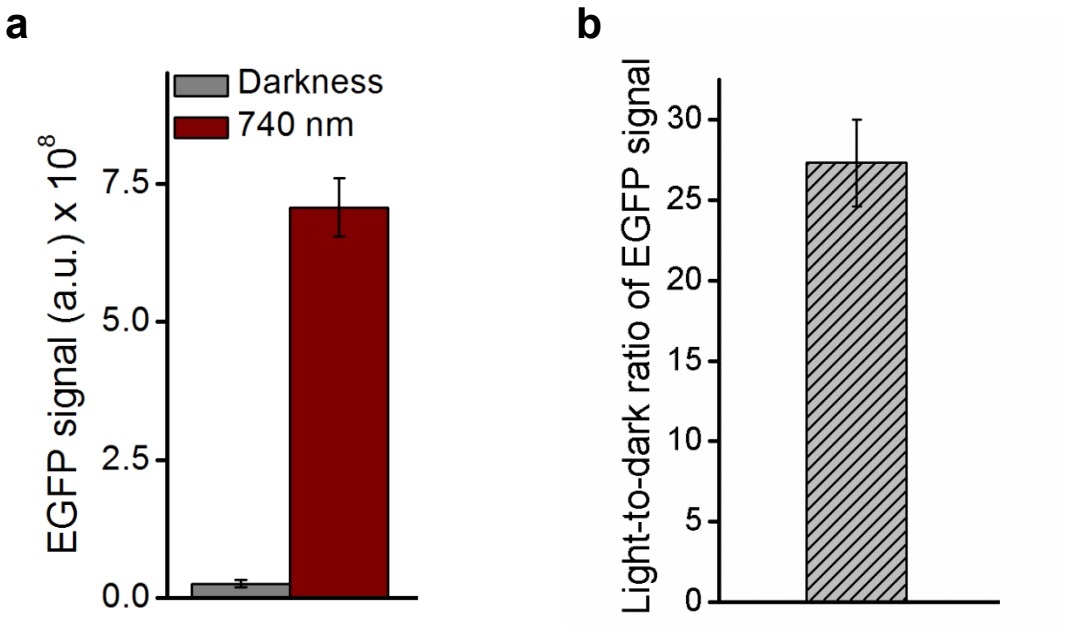

(**a**) Light-induced expression of EGFP from the pTRE-Tight-EGFP reporter plasmid. EGFP signal was detected in HeLa cells bearing BphP1-mCherry-TetR co-transfected with pCMV-104 and pTRE-Tight-EGFP plasmids. Cells were kept in darkness (gray) or under 740/25 nm light (dark red) for 48 h and analyzed using flow cytometry ($n=5x10^4$) (n=3, error bars are s.e.m.). (**b**) Light-to-dark ratio of the EGFP signals shown in (a).

Supplementary Figure 10.

Dose–response curves for light-induced SEAP expression for BphP1–PpsR2 and PhyB–PIF6 systems.

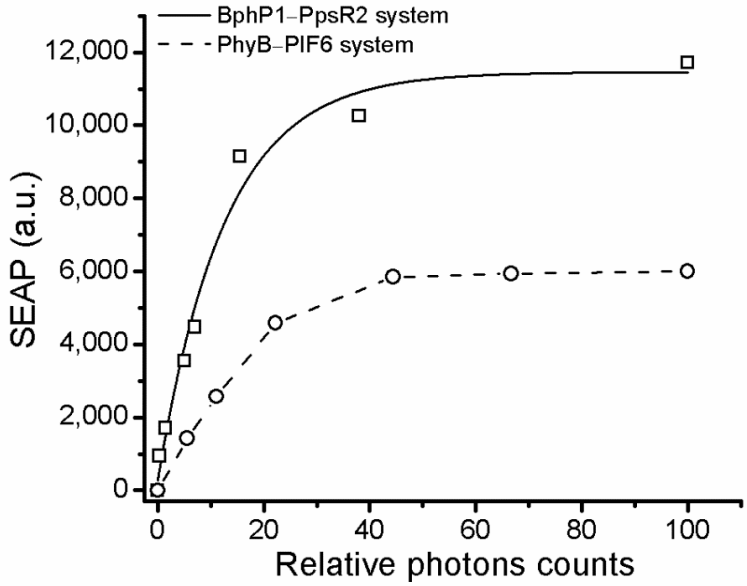

SEAP signal was detected in HeLa cells with BphP1-mCherry-TetR, pTRE-Tight-SEAP and pCMV-104 plasmids (squares) and in HeLa cells with pTRE-Tight-SEAP plasmid and pKM022 plasmid[2], supplemented with 15 μM of phycocyanobilin (circles). Cells were kept in darkness or illuminated with 740/25 nm light for the BphP1–PpsR2 system or illuminated with 660/20 nm light in a case of the PhyB–PIF6 system.

Supplementary Figure 11.

Comparison of penetration depth of far-red and NIR light in different mammalian tissues.

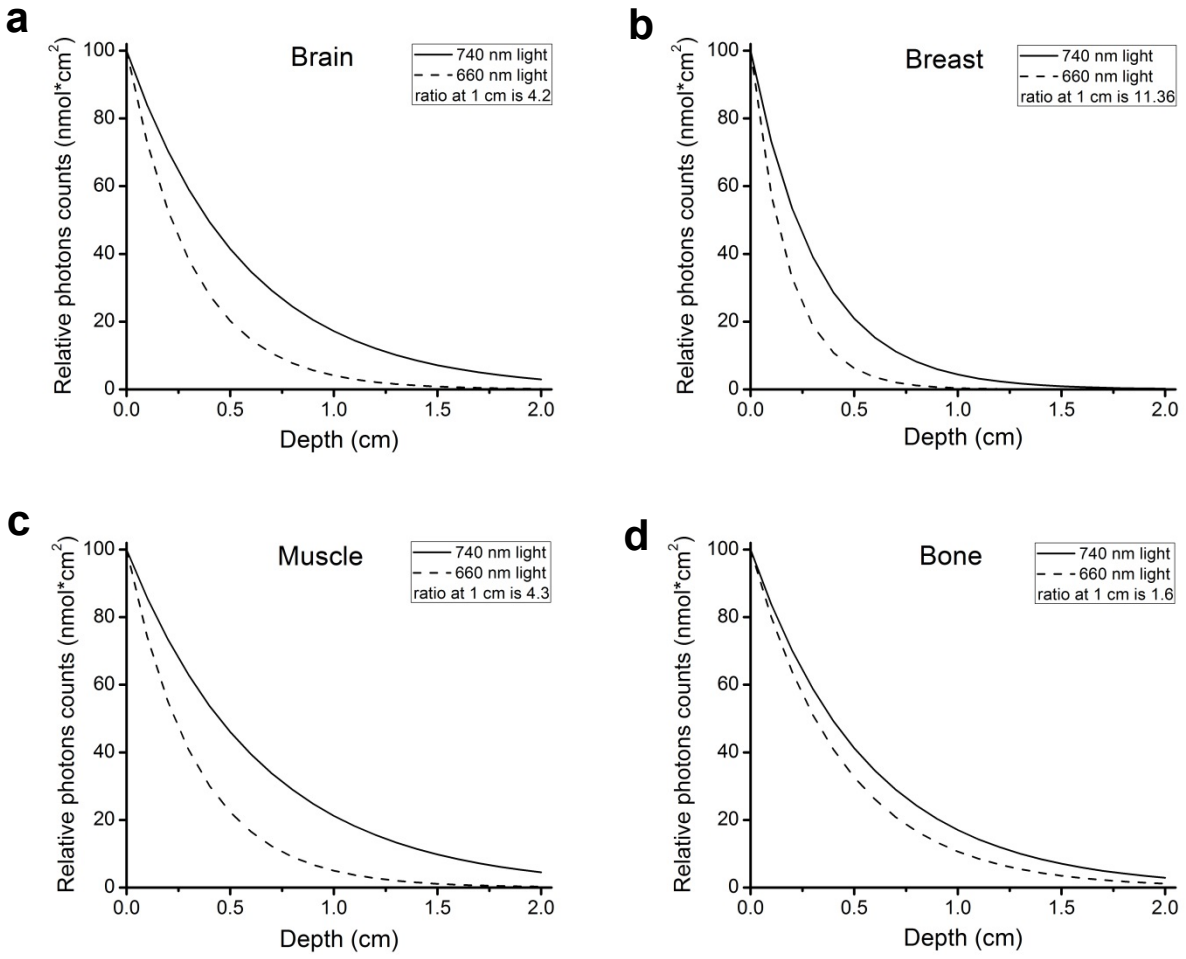

Dependences of the photon counts at 660 nm (dashed line) and 740 nm (solid line) wavelengths on the depth of penetration for (a) mammalian brain, (b) breast, (c) muscle and (d) bone tissues. See **Supplementary Note** for more details.

Supplementary Figure 12.

Estimated efficiency of the SEAP light-induced expression for the BphP1–PpsR2 and PhyB–PIF6 systems at various depths in a muscle tissue.

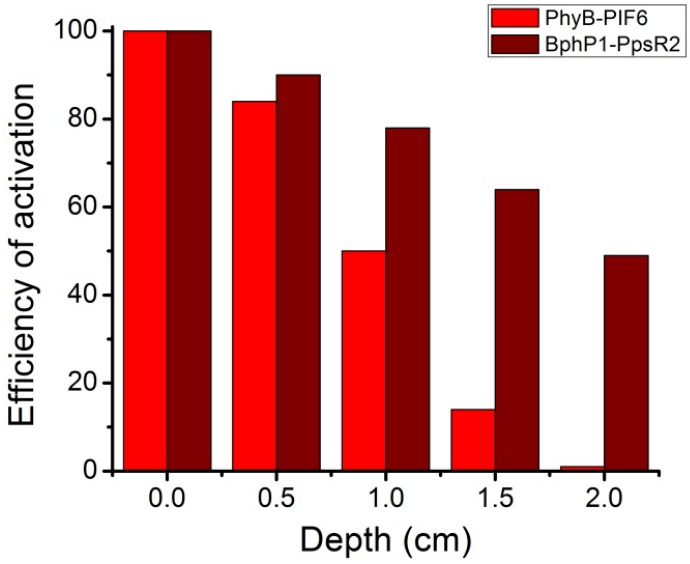

Dependence of the relative activation efficiency of the BphP1–PpsR2 and PhyB–PIF6 systems on the depth of a muscle tissue. The systems are activated with 740 nm (dark red) and 660 nm (red) light, respectively. Calculation of the relative efficiencies was based on the light-sensitivity measurements for both optogenetic systems (**Supplementary Fig. 10**) and on the light-attenuation properties of a mammalian muscle tissue (**Supplementary Fig. 11c)**.

Supplementary Figure 13.

Blue light-induced expression of Rluc8 in HeLa cells transfected with LightON system.

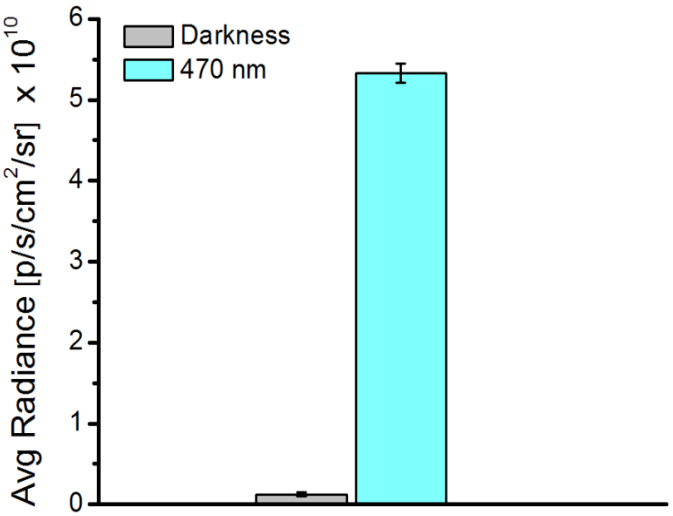

The Rluc8 bioluminescence signal was detected in HeLa cells transiently transfected with the pGAVPO plasmid[3] and with the pU5-Rluc8 plasmid in a 1:1 ratio. 10 h after the transfection cells were continuosly illuminated with 470/15 nm light (1 mW cm^{-2}) or remained in darkness for 48 h (n=3, error bars are s.e.m.).

Supplementary Figure 14.

Spectral compatibility of LightON and BphP1–PpsR2 systems.

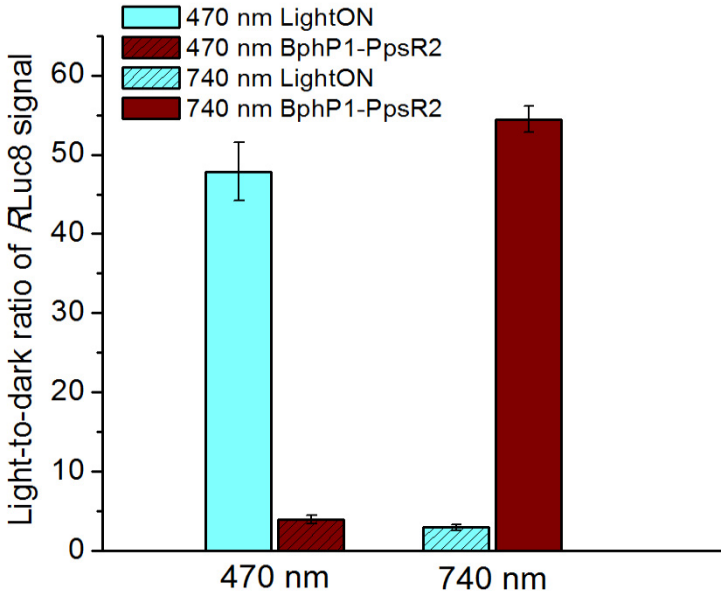

The light-to-dark ratio of Rluc8 bioluminescence signal detected in HeLa cells co-transfected with the pGAVPO plasmid[3] and with the pU5-Rluc8 plasmid in a 1:1 ratio (blue columns) and in HeLa cells expressing BphP1-mCherry-TetR co-transfected with the pTRE-Tight-Rluc8 and pCMV-104 plasmids with a 1:5 ratio (dark red columns). After the transfection, the cells were continuously illuminated for 48 h with either 470/15 nm (0.5 mW cm^{-2}) or 740/20 light (0.5 mW cm^{-2}) or remained in darkness (n=3, error bars are s.e.m.).

Supplementary Figure 15.

Blue light-induced transcription activation in mice livers hydrodynamically transfected with high amounts of LightON plasmids.

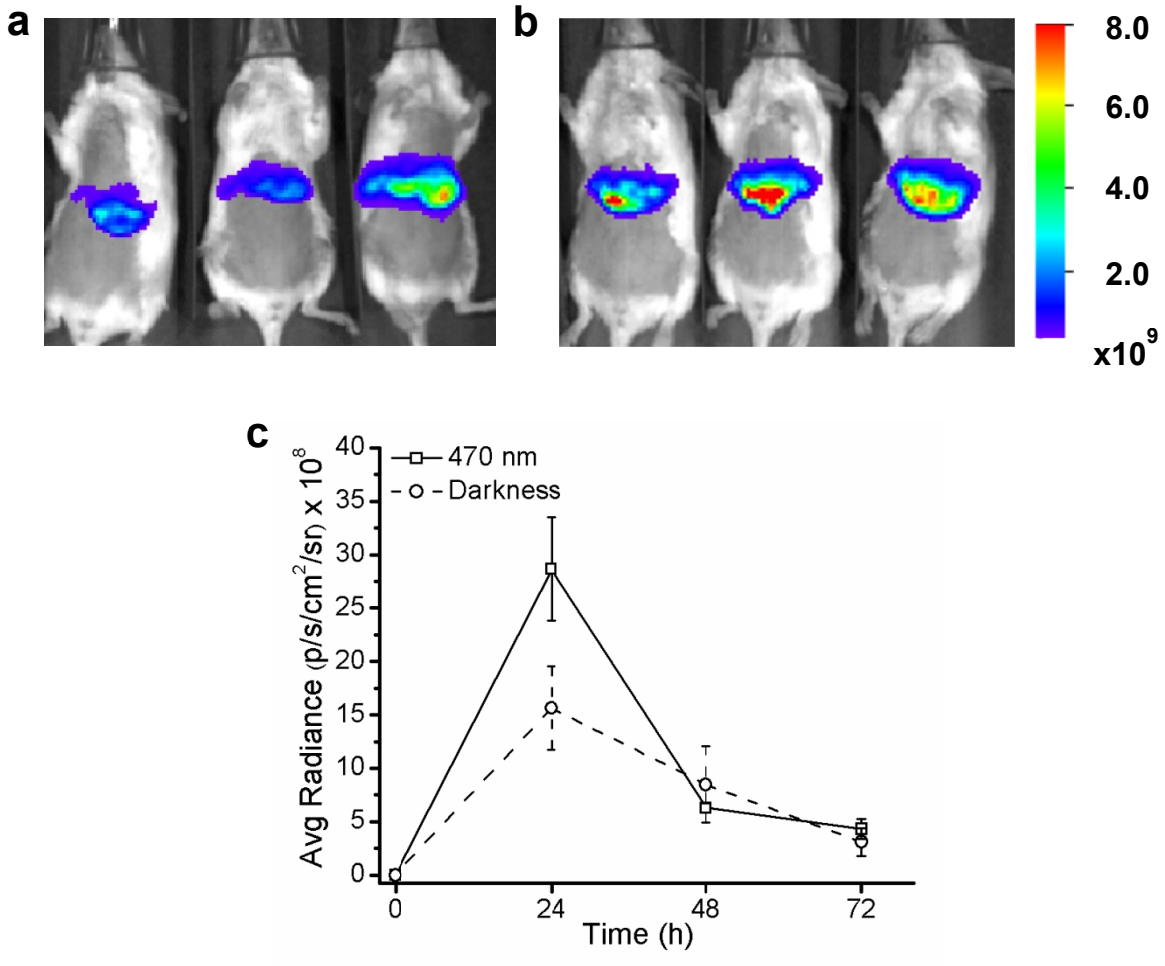

Rluc8 bioluminescence signals detected in mice after hydrodynamic co-transfection of the livers with the pGAVPO plasmid[3] (10 µg) and the pU5-Rluc8 reporter plasmid (300 µg). Mice kept (a) in darkness or (b) illuminated with 470/15 nm light of 5 mW cm^{-2} for 24 h are shown. (**c**) The kinetics of the Rluc8 expression in mice kept in darkness or illuminated with 470/15 nm light at 5 mW cm^{-2} continuously for 72 h is quantified (n=3; error bars are s.e.m.). The color bar in (a) and (b) indicates the total bioluminescence radiance in [photons s^{-1} cm^{-2} $steradian^{-1}$].

Supplementary Note

Optical properties of mammalian tissues differ from type to type, and should be regarded as a complex function of different factors. A total absorption of a tissue depends on several parameters, such as an oxygenation degree of hemoglobin, a blood volume, a water content, a fat content, a concentration of endogenous chromophores (bilirubin, melanin, carotene, etc.), a Rayleigh light scattering and a Mie light scattering[4]. The tissue optical properties are usually described in terms of three parameters: a scattering coefficient, μ_s, an absorption coefficient, μ_a, and a scattering anisotropy factor, g.

The absorption and scattering coefficients are defined as the probability of absorption or scattering, respectively, per a path-length unit. The third parameter is the scattering distribution in a turbid media, described by the anisotropy factor and obtained by computing the mean cosine of the scattering angle. The value of g, in a scale from −1 to 1, characterizes the direction of the scattering. In most biological tissue, the g value ranges from 0.70 to 0.99, indicating that photons are preferably scattered in the forward direction. Using g factor we can compute a reduced scattering coefficient, which takes into account the anisotropy of scattering in a studied tissue:

$$\mu_s' = (1 - g)\mu_s \quad (1)$$

In a reality, when samples of a bulk tissue are analyzed, the above-mentioned parameters are difficult to evaluate, as these situations are characterized by the occurrence of multiple scattering and absorption events. As the consequence, to characterize optical properties of thick samples another parameter is utilized. An effective attenuation coefficient, μ_{eff}, is equal to an inverse of the attenuation length at which the incident spatial irradiance is attenuated by factor of $1/e$ (~37%). The relation between μ_{eff}, μ_a and μ'_s is defined as

$$\mu_{eff} = \sqrt{3\mu_a(\mu_a + \mu_s')} \quad (2)$$

The optical properties of different mammalian tissues have been studied by many research groups, and the μ_a and μ'_s coefficients were experimentally determined for many tissues[5-10]. Thus, it is possible to calculate μ_{eff} using equation (2).

Generally, a relation between absorbed light energy and pathway through which light travels is defined by Beer-Lambert law for thick layers:

$$I(d) = I_0 e^{(-\mu_{eff} d)} \quad (3)$$

where I_0 is the initial light intensity, μ_{eff} is the effective attenuation coefficient of tissue at wavelength λ, and d is the path length of light through the sample.

Nature Methods: doi:10.1038/nmeth.3864

Using equation (2) and (3) we have calculated and plotted the dependence of relative photon counts for far-red (660 nm) and NIR (740 nm) light on the depth of penetration for 4 mammalian tissues, such as brain (μ_{eff}^{660} =3.2, μ_{eff}^{740} =1.76)[9], breast (μ_{eff}^{660} =5.5, μ_{eff}^{740} =3.13)[10], muscle (μ_{eff}^{660} =3, μ_{eff}^{740} =1.55)[5] and bone (μ_{eff}^{660} =2.24, μ_{eff}^{740} =1.77)[10] (**Supplementary Fig. 14**). Substantial difference in penetration between 740 nm and 660 nm light at 1 cm depth is observed for the brain and muscle tissues where NIR light penetrates 4-fold more efficiently. The largest difference, ~11-fold, in penetration between 740 nm and 660 nm at 1 cm depth is observed for the breast tissue (**Supplementary Fig. 14b**). This is because of the high level of fat and water content that resulted in the higher μ'_s for 660 nm light.

Overall, our considerations are consistent with the results published earlier[11]. Importantly, in the NIR tissue transparency window the depth of light penetration is highly affected by light-scattering phenomenon: the absorption coefficients for many tissues within 650-900 nm range are ~10-fold lower than the light-scattering coefficients[10].

Supplementary References

1. Shcherbakova, D.M. & Verkhusha, V.V. Near-infrared fluorescent proteins for multicolor in vivo imaging. *Nat Methods* **10**, 751-754 (2013).
2. Muller, K. et al. A red/far-red light-responsive bi-stable toggle switch to control gene expression in mammalian cells. *Nucleic Acids Res* **41**, e77 (2013).
3. Wang, X., Chen, X. & Yang, Y. Spatiotemporal control of gene expression by a light-switchable transgene system. *Nat Methods* **9**, 266-269 (2012).
4. Jacques, S.L. Optical properties of biological tissues: a review. *Phys Med Biol* **58**, R37-61 (2013).
5. Xia, J.J., Berg, E.P., Lee, J.W. & Yao, G. Characterizing beef muscles with optical scattering and absorption coefficients in VIS-NIR region. *Meat Sci* **75**, 78-83 (2007).
6. Marquez, G., Wang, L.V., Lin, S.P., Schwartz, J.A. & Thomsen, S.L. Anisotropy in the absorption and scattering spectra of chicken breast tissue. *Appl Opt* **37**, 798-804 (1998).
7. Grabtchak, S., Montgomery, L.G. & Whelan, W.M. Optical absorption and scattering properties of bulk porcine muscle phantoms from interstitial radiance measurements in 650-900 nm range. *Phys Med Biol* **59**, 2431-2444 (2014).
8. Simpson, C.R., Kohl, M., Essenpreis, M. & Cope, M. Near-infrared optical properties of ex vivo human skin and subcutaneous tissues measured using the Monte Carlo inversion technique. *Phys Med Biol* **43**, 2465-2478 (1998).
9. Driver, I., Lowdell, C.P. & Ash, D.V. In vivo measurement of the optical interaction coefficients of human tumours at 630 nm. *Phys Med Biol* **36**, 805-813 (1991).
10. Sandell, J.L. & Zhu, T.C. A review of in-vivo optical properties of human tissues and its impact on PDT. *J Biophotonics* **4**, 773-787 (2011).
11. Lecoq, J. & Schnitzer, M.J. An infrared fluorescent protein for deeper imaging. *Nat Biotechnol* **29**, 715-716 (2011).